Automatica 98 (2018) 223–238

Contents lists available at ScienceDirect

Automatica

journal homepage: www.elsevier.com/locate/automatica

Balancing and suppression of oscillations of tension and cage in dual-cable mining elevators☆

Ji Wang [a,b,c], Yangjun Pi [a,c,*], Miroslav Krstic [b]

[a] State Key Laboratory of Mechanical Transmission, Chongqing University, Chongqing 400044, China
[b] Department of Mechanical and Aerospace Engineering, University of California, San Diego, La Jolla, CA 92093-0411, USA
[c] College of Automotive Engineering, Chongqing University, Chongqing 400044, China

ARTICLE INFO

Article history:
Received 7 November 2017
Received in revised form 21 May 2018
Accepted 9 August 2018
Available online 26 September 2018

Keywords:
Distributed parameter systems
Hyperbolic PDEs
PDE–ODE
Time-varying system
Backstepping

ABSTRACT

Dual-cable mining elevator has advantages in the transportation of heavy load to a large depth over the single cable elevator. However challenges occur when lifting a cage via two parallel compliant cables, such as tension oscillation inconformity between two cables and the cage roll, which are important physical variables relating to the fatigue fracture of mining cables. Mining elevator vibration dynamics are modeled by two pairs of 2×2 heterodirectional coupled hyperbolic PDEs on a time-varying domain and all four PDE bottom boundaries are coupled at one ODE. We design an output feedback boundary control law via backstepping to exponentially stabilize the dynamic system including the tension oscillation states, tension oscillation error states and the cage roll states. The control law is constructed with the estimated states from the observer formed by available boundary measurements. The exponential stability of the closed-loop system is proved via Lyapunov analysis. Effective suppression of tension oscillations, reduction of inconformity between tension oscillations in two cables, and balancing the cage roll under the proposed controller are verified via numerical simulation.

© 2018 Elsevier Ltd. All rights reserved.

1. Introduction

Mining cable elevator: In mining exploitation, a cable elevator, which is used to transport the cargo and miners between the ground and the working platform underground, represents an indispensable equipment. Cable plays a vital role in the deep mining elevators because its advantages of low bending and torsional stiffness, resisting relatively large axial loads, are helpful to the heavy load and large depth transportation. However, the compliance property or stretch and contract abilities of cables, tend to cause mechanical vibrations, which lead to premature fatigue fracture due to tension oscillations. Therefore, the importance of suppressing the tension oscillations cannot be overestimated, considering the safety of personnel and profitability.

Single-cable mining cable elevator: A common arrangement in elevator systems, referred to a single-drum system (Wang, Koga, Pi, & Krstic, 2018), comprises a driving winding drum, a steel wire cable, a head sheave, and a cage. The important feature of this systems is that the cable is of a time-varying length. The vibration dynamic model is a wave PDE–ODE coupled system on a time-varying domain. Suppressing the axial vibrations distributed in the cable and attenuating a disturbance at the cage through the control force applied at the head sheave in such a single cable elevator have been achieved in Wang, Koga et al. (2018) and Wang, Tang, Pi, and Krstic (2018) respectively.

Dual-cable mining cable elevator: For the operation at a greater depth, such as over 2000 m, and carrying a heavier load, the single cable elevator is not suitable. Because a very thick cable is required to bear the heavy load and such a cable, at high bending, causes problems in the winding on the winder drum. A dual-cable mining elevator (Wang, Pi, Hu, & Gong, 2017) shown in Fig. 1 is proposed to solve this problem, where the requirement of a very thick cable can be removed because two cables tow the cage. However, the imbalance problem such as cage roll frequently appears in the dual-cable elevator, which is shown in Fig. 1 where taut cables are used as flexible guide rails (Wang, Pi et al., 2017) because traditional steel rails are with high cost of manufacture and installment in deep mines. Cage roll would increase the error of oscillation tensions between two cables, and enlarge the oscillation amplitude of the tension in cables, which accelerates premature fatigue and requires inspections and costly repairs. One feasible

☆ This work is supported by the National Basic Research Program of China (973) [2014CB049404]. The material in this paper was not presented at any conference. This paper was recommended for publication in revised form by Associate Editor Angelo Alessandri under the direction of Editor Thomas Parisini.

* Corresponding author at: State Key Laboratory of Mechanical Transmission, Chongqing University, Chongqing 400044, China.
E-mail addresses: wangji@cqu.edu.cn (J. Wang), cqpp@cqu.edu.cn (Y. Pi), krstic@ucsd.edu (M. Krstic).

https://doi.org/10.1016/j.automatica.2018.09.027
0005-1098/© 2018 Elsevier Ltd. All rights reserved.

and possible arrangement to balance the cage roll and suppress the tension oscillations in cables of the dual-cable mining elevator is applying additional control forces through actuators at floating head sheaves shown in Fig. 1. However, designing control forces applied at top boundaries of the cables to balance a cage coupled with the bottom boundaries through two time-varying length compliant cables and suppress the tension oscillations in cables is a challenging task, which has heretofore remained unsolved.

Control of heterodirectional coupled hyperbolic PDE systems: Mathematically, the vibration dynamic model of a dual-cable mining elevator can be abstractly described by two pairs of 2×2 heterodirectional coupled hyperbolic PDEs on a time-varying domain and all four PDE bottom boundaries are coupled at one ODE, which is reversibly converted from the system consisting of two wave PDEs coupled with one ODE on a time-varying domain using the Riemann coordinates. We set out to exponentially stabilize such a strongly coupled and time-varying distributed parameter system in the sense of H^1 norm via the output control design at one boundary.

Some theoretical results on controlling coupled hyperbolic PDEs systems have emerged over the last decade. Backstepping boundary stabilization and state estimation of a 2×2 linear hyperbolic system were considered in Vazquez, Krstic, and Coron (2011). A full-state control law was proposed to exponentially stabilize 2×2 hyperbolic linear systems in Coron, Vazquez, Krstic, and Bastin (2013). Stabilization of 2×2 first-order hyperbolic linear PDEs with uncertain parameters was solved via adaptive control in Anfinsen and Aamo (2017a, 2018) and Yu, Vazquez, and Krstic (2017) using identifier or swapping design. Backstepping design of output feedback regulators that achieve regulation in finite time for boundary controlled linear 2×2 hyperbolic systems was presented in Deutscher (2017b). Moreover, stabilization of $n + 1$ coupled first-order hyperbolic linear PDEs was considered in Di Meglio, Vazquez, and Krstic (2013). A control problem of a first-order hyperbolic linear PDE general system where the number of PDEs in either direction is arbitrary was solved in Hu, Di Meglio, Vazquez, and Krstic (2016). Some results about control of linear hyperbolic coupled PDEs cascaded with ODEs were also presented. Output feedback control law of a 2×2 linear hyperbolic system cascaded with an ODE acting as disturbance dynamics was developed in Aamo (2013) and Anfinsen and Aamo (2015). An observer design for a class of hyperbolic PDE–ODE cascade systems with a boundary measurement was presented in Hasan, Aamo, and Krstic (2016). Controller and observer design for a $n \times m$ linear hyperbolic system cascaded with an ODE was proposed in Anfinsen and Aamo (2017b). The output regulation problem for general linear heterodirectional hyperbolic systems with spatially-varying coefficients, where disturbances described by a cascaded ODE at both boundaries, distributed in-domain or at the output to be controlled, was solved in Deutscher (2017c). The research on control of the coupled linear hyperbolic PDE systems coupled with an ODE at the non-controlled boundary is limited. In a very recent result, the state-feedback boundary control design of a 2×2 linear hyperbolic PDE–ODE coupled system with non-local terms was solved in Su, Wang, and Krstic (2018). The state-feedback stabilization of a general linear hyperbolic PDE–ODE coupled system was considered in Di Meglio, Bribiesca, Hu, and Krstic (2018), where an ODE was stabilized through compensating linear coupled hyperbolic PDEs on a fixed domain in the actuating path. An observer-based output feedback controller with anti-collocated measurements was proposed to stabilize general linear heterodirectional hyperbolic PDE–ODE systems with spatially varying coefficients in Deutscher, Gehring, and Kern (2018).

Main contribution:

(1) We suppress the tension oscillations of two cables and the cage roll in an ascending/descending mining elevator, where the two cables with in-domain viscous damping are coupled at the moving cage. It is developed from our previous work (Wang, Koga et al., 2018; Wang, Tang et al., 2018) where the vibration suppression of a single-cable ascending mining elevator neglecting the cable in-domain viscous damping is considered. The challenges arise when the in-domain viscous damping is included and both ascending/descending motions are taken into account, because the internal coupling (Roman, Bresch-Pietri, Prieur, & Sename, 2016) is introduced and the sign of the derivative of the time-varying domain affects Lyapunov stability analysis. Suppression of tension oscillations also makes the task harder than vibration suppression (Wang, Koga et al., 2018; Wang, Tang et al., 2018) because, in addition to the exponential stability result in the sense of $\|u_x(\cdot,t)\|^2+\|u_t(\cdot,t)\|^2$, the exponential stability estimate $\|u_{xx}(\cdot,t)\|^2+\|u_{xt}(\cdot,t)\|^2$ should be produced.

(2) Suppression of tension oscillations in the dual-cable mining elevator can be mathematically described as exponential stabilization of two pairs of 2×2 heterodirectional hyperbolic systems with source terms on a time-varying domain, and all hyperbolic PDEs coupled with an ODE in the boundary anti-collocated with the control input. The related theoretical results in Anfinsen and Aamo (2017b), Anfinsen, Diagne, Aamo, and Krstic (2017) and Deutscher (2017a) only solve the problem of general coupled heterodirectional hyperbolic PDEs cascaded with ODEs on fixed domains.

(3) Different from the very recent results in Deutscher et al. (2018) and Di Meglio et al. (2018) which stabilize the general heterodirectional hyperbolic PDE–ODE coupled system on a fixed domain in L^2 sense, we stabilize a 2×2 heterodirectional hyperbolic PDE–ODE coupled system on a time-varying domain in H^1 sense.

(4) In the field of control applications, this is the first control design to suppress roll and axial vibrations of a moving object anti-collocated with the control input through two parallel compliant cables of time-varying length, whose tension oscillations are suppressed to zero simultaneously.

Organization: The rest of the paper is organized as follows. The dynamics of a dual-cable mining elevator with material damping of the steel cables is presented in Section 2. A state observer is designed and proved exponentially convergent to the plant in Section 3. An observer-based output feedback controller is designed via backstepping in Section 4. The exponential stability of the closed-loop system and the exponential convergence of the control inputs are proved in Section 5. The simulation results are provided in Section 6. The conclusion and future work are presented in Section 7.

Notation: Throughout this paper, the cable number (1,2) in the dual-cable mining elevator are denoted as the subscripts: $i = 1, 2$ or $j = 2, 1, j \neq i$. The partial derivatives and total derivatives are denoted as: $f_x(x,t) = \frac{\partial f}{\partial x}(x,t)$, $f_t(x,t) = \frac{\partial f}{\partial t}(x,t)$, $\gamma'(x) = \frac{d\gamma(x)}{dx}$, $\dot{X}(t) = \frac{dX(t)}{dt}$.

2. Problem formulation

2.1. Dynamics of dual-cable mining elevators

The actual displacement $z_i^*(x,t), i = 1, 2$ of each point in the cables can be considered as the sum of the translation $l(t)$

in the equal rigid-body model and the additional axial vibrations $u(x,t)$, $v(x,t)$ of the compliant ones, i.e., $z_1^*(x,t) = l(t) + u(x,t)$, $z_2^*(x,t) = l(t) + v(x,t)$. $u(x,t)$, $v(x,t)$ are referred to a moving coordinate system associated with the axial motion $l(t)$ where the origin is located at the cage. Using Hamilton's principle and through the derivation and simplification similar in Wang, Koga et al. (2018), vibration dynamics $u(x,t)$, $v(x,t)$ can be built as

$$\dot{X}(t) = AX(t) + B[u_x(0,t), v_x(0,t)]^T, \tag{1}$$

$$u_{tt}(x,t) = qu_{xx}(x,t) - cu_t(x,t), \tag{2}$$

$$v_{tt}(x,t) = qv_{xx}(x,t) - cv_t(x,t), \tag{3}$$

$$C_3X(t) + C_4X(t)l_1 = u_t(0,t), \tag{4}$$

$$C_3X(t) - C_4X(t)l_1 = v_t(0,t), \tag{5}$$

$$u_x(l(t),t) = U_1(t),\ v_x(l(t),t) = U_2(t), \tag{6}$$

$x \in [0, l(t)], t \in [0,\infty)$, where (2)–(3) are telegraph equations (Gugat, 2014). Matrices A and $B = [\bar{B}_1, \bar{B}_2]$ are

$$A = \begin{pmatrix} 0 & 0 & 1 & 0 \\ 0 & 0 & 0 & 1 \\ 0 & 0 & \frac{-c_d}{M} & 0 \\ 0 & 0 & 0 & \frac{-c_a}{J_c} \end{pmatrix}, B = E_A \begin{pmatrix} 0 & 0 \\ 0 & 0 \\ \frac{-1}{M} & \frac{-1}{M} \\ \frac{-1}{J_c} & \frac{1}{J_c} \end{pmatrix}. \tag{7}$$

M denotes the mass of the load. $C_3 = [0,0,1,0]$ and $C_4 = [0,0,0,1]$. $l(t)$ describes the time-varying length of the cables. J_c is the moment of inertia of the cage. $q = \frac{E\times A_a}{\rho}$ where E, A_a and ρ are Young's modulus, the cross-sectional area and linear density of the cables respectively. c_d and c_a denote the damping coefficients of cage axial and roll motion respectively. $c = \frac{\bar{c}}{\rho}$ where $\bar{c}$ is the material damping coefficient of the steel cables. l_1 is the cage dimension shown in Fig. 1.

The PDE states $u(x,t)$, $v(x,t)$ in (2)–(3) describe the axial vibration displacements of the distributed points in cable 1 and cable 2 respectively. $u_x(x,t)$ and $v_x(x,t)$ denote the distributed strain in the cables and the tension oscillations are represented as $E_Au_x(x,t)$ and $E_Av_x(x,t)$ where the constant $E_A = E \times A_a$. $E_Au_x(0,t)$ and $E_Av_x(0,t)$ denoting forces acting on the cage drive the ODE dynamics (1), where the ODE state $X(t) = [y(t), \theta(t), \dot{y}(t), \dot{\theta}(t)]^T$ describes the cage dynamics. $y(t)$, $\dot{y}(t)$ are the axial vibration displacement and velocity of the centroid of the cage, and $\theta(t)$, $\dot{\theta}(t)$ are the cage roll angle and roll rate around the axis which is vertical to the door and through the centroid of the cage. (4)–(5) describe the velocity relationship between the cage and the bottom boundaries of the two cables. (6) comes from $E_Au_x(l(t),t) = U_{1v}(t)$ and $E_Av_x(l(t),t) = U_{2v}(t)$ with the definition of $U_{1v}(t) = E_AU_1(t)$ and $U_{2v}(t) = E_AU_2(t)$, using which the two actual control forces at the two floating sheaves $U_{1v}(t)$, $U_{2v}(t)$ can be obtained by $U_1(t)$, $U_2(t)$ to be designed in this paper.

Remark 1. Axial motion dynamics $l(t)$ is regulated by a separate controller $U_a(t)$ at the drum. We ignore the effect of the vibration dynamics on the motion dynamics because the vibration displacements $u(x,t)$, $v(x,t)$ are much smaller than the hoisting motion $l(t)$ between 2000 m under ground and the surface platform. We can then consider that $l(t)$ state in an independent ODE (motion dynamics) driven by $U_a(t)$ is the known hosting trajectory, and focus on the control design $U_i(t)$ at the floating head sheave for the PDE vibration dynamics (1)–(6), where $l(t)$ acts as a known time-varying domain.

Remark 2. We conduct the control design based on a more general model where the damping coefficients c_a, c_d, c in the model (1)–(6) are arbitrary. In other words, these damping coefficients can be damped (> 0), undamped ($= 0$), or even anti-damped (< 0).

Assumption 1. $l(t) \in C^2(0,\infty)$. $l(t)$ is bounded: $0 < l(t) \le L$, $\forall t \ge 0$, where L denotes the total length of the cable.

Assumption 2. Velocity $\dot{l}(t)$ of the moving boundary is bounded by

$$|\dot{l}(t)| \le \bar{v}_{\max} < \sqrt{q}, \tag{8}$$

where $\bar{v}_{\max}$ is the maximum velocity of the mining cable elevator.

Note: In the mining cable elevator, the value of $\sqrt{q} = r/\rho = 7.5 \times 10^3$ is much larger than the value of the maximum hoisting velocity $\bar{v}_{\max} = 16.25$ m/s, thus $\bar{v}_{\max} < \sqrt{q}$. Moreover, according to the conclusion in Gugat (2007a, b), the fact that the derivative of the moving boundary $\dot{l}(t)$ is smaller than the wave speed $\sqrt{q}$ allows to prove a well-posedness result for the initial boundary value problem (1)–(6). Since the wave speed in the cables is usually much larger than the speed of the cage the assumption usually holds in the applications.

In addition to suppression of oscillations of tension in each cable, that of tension oscillation error between two cables is required via controller design as well. Therefore, the error between tension oscillations in two cables should be built to design the controller. Define a new system-(e,s) as

$$e(x,t) = v(x,t) - u(x,t), \tag{9}$$

$$s(x,t) = v(x,t) + u(x,t), \tag{10}$$

where $E_Ae_x(x,t) = E_Av_x(x,t) - E_Au_x(x,t)$ is the error of oscillations of tension between two cables and $E_As_x(x,t)$ is the total oscillations of tension in two cables.

The control objectives are

- Physically, suppress the oscillations of tension in each cable as soon as possible. Theoretically, the closed-loop system-(u,v) is exponentially stable in the sense of terms including $\|u_{xx}(\cdot,t)\| + \|v_{xx}(\cdot,t)\|$, where the exponential decay rate can be chosen.
- Physically, reduce the error of oscillations of tension between two cables as fast as possible. Theoretically, the system-(e,s) is exponentially stable in the sense of terms including $\|e_{xx}(\cdot,t)\| + \|s_{xx}(\cdot,t)\|$, where the exponential decay rate can be chosen.
- Physically, suppress the axial vibration displacement $y(t)$ and roll angle $\theta(t)$ of the cage as fast as possible. Theoretically, $|X(t)|$ is exponentially convergent to zero when $t \to \infty$, where the exponential decay rate can be chosen.

Note that $\|u(\cdot,t)\|$ is a compact notation for $\sqrt{\int_0^{l(t)} u(x,t)^2 dx}$.

2.2. Reformulation of the system in Riemann variables

In order to reduce the time derivative order of the plant to facility control design, we introduce the following Riemann coordinates,

$$z_1(x,t) = s_t(x,t) - \sqrt{q}s_x(x,t), \tag{11}$$

$$w_1(x,t) = s_t(x,t) + \sqrt{q}s_x(x,t), \tag{12}$$

$$z_2(x,t) = e_t(x,t) - \sqrt{q}e_x(x,t), \tag{13}$$

$$w_2(x,t) = e_t(x,t) + \sqrt{q}e_x(x,t). \tag{14}$$

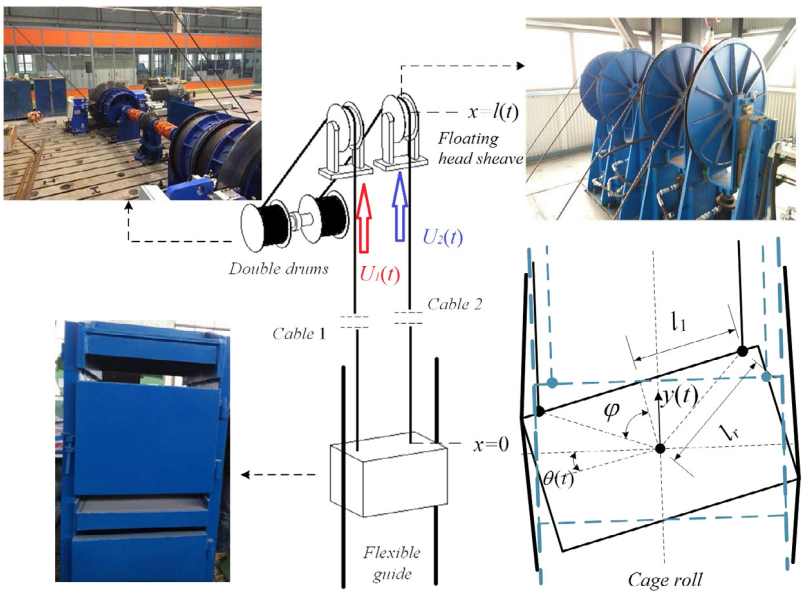

Fig. 1. Diagram and the prototype of a dual-cable mining elevator with flexible guide rails.

Considering (9)–(10), the system (1)–(6) is rewritten as

$$\dot{X}(t) = \bar{A}X(t) + \sum_{i=1}^{2} \frac{B_i}{\sqrt{q}} w_i(0,t), \tag{15}$$

$$z_{it}(x,t) = -\sqrt{q} z_{ix}(x,t) - \frac{c}{2}(z_i(x,t) + w_i(x,t)), \tag{16}$$

$$w_{it}(x,t) = \sqrt{q} w_{ix}(x,t) - \frac{c}{2}(z_i(x,t) + w_i(x,t)), \tag{17}$$

$$z_i(0,t) = D_i X(t) - w_i(0,t), \tag{18}$$

$$w_i(l(t),t) = z_i(l(t),t) + 2\sqrt{q} U_{ei}(t), \tag{19}$$

$x \in [0, l(t)]$, $t \in [0, \infty)$, where $i = 1, 2$, $\bar{A} = A - \frac{2B_1}{\sqrt{q}} C_3 + \frac{2B_2}{\sqrt{q}} C_4 l_1$, $D_1 = 4C_3$, $D_2 = -4l_1 C_4$, $B_1 = (\bar{B}_1 + \bar{B}_2)/2$, $B_2 = (\bar{B}_2 - \bar{B}_1)/2$, and

$$U_{e1}(t) = U_2(t) + U_1(t), \tag{20}$$

$$U_{e2}(t) = U_2(t) - U_1(t). \tag{21}$$

We have now two pairs of time-varying domain heterodirectional transport PDEs $w_i(x,t), z_i(x,t), i = 1, 2$. (16)–(19) with source terms result from in-domain damping. $w_i(x,t), z_i(x,t)$ are coupled with an ODE (15) at the non-collocated boundary. The first transport PDE w_i with actuation on one boundary (19), and driving the ODE (15) through its second boundary. The second transport PDE z_i is backward and driven by the state of the ODE $X(t)$ and the boundary states $w_i(0,t)$ in (18). The diagram describing this plant dynamics is shown in Fig. 2.

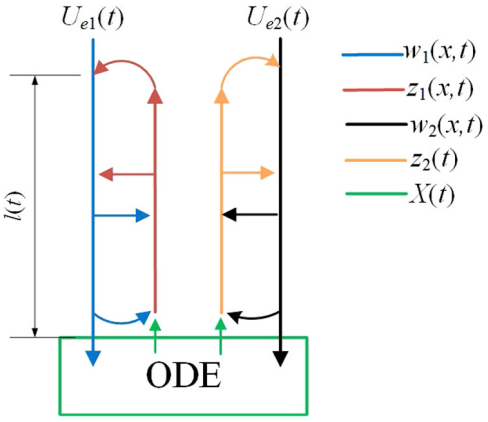

Fig. 2. Diagram of the plant dynamics (15)–(19).

Remark 3. Different from Roman, Bresch-Pietri, Cerpa, Prieur, and Sename (2016) and Roman, Bresch-Pietri, Prieur et al. (2016) which achieve the robust result to a small positive in-domain damping coefficient in wave PDEs with in-domain viscus damping terms, in our case the in-domain damping coefficient c can be arbitrary constants.

3. Observer design

In order to estimate the distributed states $z_i(x,t), w_i(x,t)$ which usually cannot be measured in practice but required in the controller, we design an observer to recover the distributed states $z_i(x,t), w_i(x,t)$ only using the available boundary measurements.

3.1. Observer structure

The available measurements in the mining cable elevator are

- Axial vibration acceleration $\ddot{y}(t)$ and roll angular acceleration $\ddot{\theta}(t)$ in the cage where accelerometers are placed. Note that measuring acceleration is the prevalent method in control of vibrating mechanical systems because accelerations are easier to measure with accelerometers than displacements or velocities (Basturk & Krstic, 2014).
- Force $E_A u_x(l(t),t)$, $E_A v_x(l(t),t)$ and velocity $u_t(l(t),t)$, $v_t(l(t),t)$ feedback signals of the serve actuators at two floating sheaves.

The observer is built as a copy of the plant (15)–(19) with some error injections,

$$\dot{\hat{X}}(t) = \bar{A}\hat{X}(t) + \sum_{f=1}^{2} \frac{B_f}{\sqrt{q}} \hat{w}_f(0,t) + \bar{L}\left((y(t) + \theta(t)) - (C_1 + C_2)\hat{X}(t)\right), \tag{22}$$

$$\hat{z}_{it}(x,t) = -\sqrt{q}\hat{z}_{ix}(x,t) - \frac{c}{2}(\hat{z}_i(x,t) + \hat{w}_i(x,t)) + \bar{\Gamma}_i(x,t)(z_i(l(t),t) - \hat{z}_i(l(t),t)), \tag{23}$$

$$\hat{w}_{it}(x,t) = \sqrt{q}\hat{w}_{ix}(x,t) - \frac{c}{2}(\hat{z}_i(x,t) + \hat{w}_i(x,t)) + \Gamma_i(x,t)(z_i(l(t),t) - \hat{z}_i(l(t),t)), \tag{24}$$

$$\hat{z}_1(0,t) = D_1X(t) - \hat{w}_1(0,t) = 4\dot{y}(t) - \hat{w}_1(0,t), \tag{25}$$

$$\hat{z}_2(0,t) = D_2X(t) - \hat{w}_2(0,t) = -4l_1\dot{\theta}(t) - \hat{w}_2(0,t), \tag{26}$$

$$\hat{w}_i(l(t),t) = z_i(l(t),t) + 2\sqrt{q}U_{ei}(t), \tag{27}$$

where $z_i(l(t),t)$ can be obtained by using $s_x(l(t),t)$, $s_t(l(t),t)$, $e_x(l(t),t)$, $e_t(l(t),t)$ which are computed by the measurements $u_x(l(t),t)$, $v_x(l(t),t)$, $u_t(l(t),t)$, $v_t(l(t),t)$. Because the acceleration sensor is more convenient to place at the cage, $y(t)$, $\theta(t)$, $\dot{y}(t)$, $\dot{\theta}(t)$ are calculated by integrating the measured accelerations $\ddot{y}(t)$, $\ddot{\theta}(t)$ with known initial conditions $y(0)$, $\theta(0)$, $\dot{y}(0)$, $\dot{\theta}(0)$. The ODE measurements $y(t)$, $\theta(t)$ and the matrix $\bar{A}$ in (22) form an observable matrix pair $(\bar{A}, C_1 + C_2)$ where $C_1 = [1,0,0,0]$, $C_2 = [0,1,0,0]$. The ODE measurements $y(t)$, $\theta(t)$, $\dot{y}(t)$, $\dot{\theta}(t)$ are used to construct a boundary condition at $x = 0$ and a Hurwitz state matrix in the ODE subsystem in the observer error system shown following, which will be helpful in searching backstepping transformations to an exponentially stable target error system to obtain the observer gains $\bar{\Gamma}_i(x,t)$, $\Gamma_i(x,t)$ in (23)–(24).

3.2. Observer error dynamics and backstepping

Defining the error system-$(\tilde{z}_i, \tilde{w}_i, \tilde{X})$ obtained from

$$(\tilde{z}_i(x,t), \tilde{w}_i(x,t), \tilde{X}(t)) = (z_i(x,t), w_i(x,t), X(t)) - (\hat{z}_i(x,t), \hat{w}_i(x,t), \hat{X}(t)), \tag{28}$$

we have the error dynamics between the plant and the observer as

$$\dot{\tilde{X}}(t) = \hat{A}\tilde{X}(t) + \sum_{i=1}^{2}\frac{B_i}{\sqrt{q}}\tilde{w}_i(0,t), \tag{29}$$

$$\tilde{z}_{it}(x,t) = -\sqrt{q}\tilde{z}_{ix}(x,t) - \frac{c}{2}(\tilde{z}_i(x,t) + \tilde{w}_i(x,t)) - \bar{\Gamma}_i(x,t)\tilde{z}_i(l(t),t), \tag{30}$$

$$\tilde{w}_{it}(x,t) = \sqrt{q}\tilde{w}_{ix}(x,t) - \frac{c}{2}(\tilde{z}_i(x,t) + \tilde{w}_i(x,t)) - \Gamma_i(x,t)\tilde{z}_i(l(t),t), \tag{31}$$

$$\tilde{z}_i(0,t) = -\tilde{w}_i(0,t), \quad \tilde{w}_i(l(t),t) = 0, \tag{32}$$

where the state matrix $\hat{A} = \bar{A} - \bar{L}(C_1 + C_2)$ in (29) is Hurwitz by choosing $\bar{L}$. We would like to design the observer gains $\bar{\Gamma}_1(x,t)$, $\bar{\Gamma}_2(x,t)$, $\Gamma_1(x,t)$, $\Gamma_2(x,t)$, to make sure the error dynamics (29)–(32) is exponentially stable.

According to Anfinsen and Aamo (2017b) and Bin and Di Meglio (2017), using the backstepping transformation

$$\tilde{z}_i(x,t) = \tilde{\alpha}_i(x,t) - \int_x^{l(t)}\bar{\phi}_i(x,y)\tilde{\alpha}_i(y,t)dy, \tag{33}$$

$$\tilde{w}_i(x,t) = \tilde{\beta}_i(x,t) - \int_x^{l(t)}\bar{\psi}_i(x,y)\tilde{\alpha}_i(y,t)dy, \tag{34}$$

we would like to convert the error dynamics (29)–(32) to the target error system as

$$\dot{\tilde{X}}(t) = \hat{A}\tilde{X}(t) + \sum_{f=1}^{2}\frac{B_f}{\sqrt{q}}\Bigg(\tilde{\beta}_f(0,t) + \int_0^{l(t)}\bar{\psi}_f(0,y)\tilde{\alpha}_f(y,t)dy\Bigg), \tag{35}$$

$$\tilde{\alpha}_{it}(x,t) = -\sqrt{q}\tilde{\alpha}_{ix}(x,t) + \int_x^{l(t)}\bar{M}_i(x,y)\tilde{\beta}_i(y,t)dy + \frac{c}{2}\tilde{\alpha}_i(x,t) - \frac{c}{2}\tilde{\beta}_i(x,t), \tag{36}$$

$$\tilde{\beta}_{it}(x,t) = \sqrt{q}\tilde{\beta}_{ix}(x,t) - \frac{c}{2}\tilde{\beta}_i(x,t) + \int_x^{l(t)}\bar{N}_i(x,y)\tilde{\beta}_i(y,t)dy, \tag{37}$$

$$\tilde{\alpha}_i(0,t) = -\tilde{\beta}_i(0,t) + \int_0^{l(t)}(\bar{\psi}_i(0,y) + \bar{\phi}_i(0,y))\tilde{\alpha}_i(y,t)dy, \tag{38}$$

$$\tilde{\beta}_i(l(t),t) = 0. \tag{39}$$

The target system (35)–(39) is a PDE-ODE cascaded system where the PDE (36)–(39) has a same structure as the target system (17)–(20) in Bin and Di Meglio (2017) and the PDE states flow into the ODE (35) with a Hurwitz state matrix $\hat{A}$.

Note that heterodirectional coupled hyperbolic PDEs (30)–(31) which include unstable sources, especially the coupled terms $\tilde{z}_i(x,t)$, $\tilde{z}_i(l(t),t)$ in (31), are intentionally converted to the target system where the coupled terms only exist in (36) while (37) only includes itself states. This motivation is also used to construct the target system of (22)–(27), which will be shown in Section 4.

The kernels $\bar{\phi}_i(x,y)$, $\bar{\psi}_i(x,y)$ in the transformation (33)–(34), $\bar{M}_i(x,y)$, $\bar{N}_i(x,y)$ in (36)–(37), and the observer gains $\bar{\Gamma}_i(x,t)$, $\Gamma_i(x,t)$ would be determined following.

3.3. Calculation of the kernels and observer gains

Substituting the transformations (33)–(34) into (30), and inserting (36), through a lengthy calculation, we have

$$\begin{aligned}&\tilde{z}_{it}(x,t) + \sqrt{q}\tilde{z}_{ix}(x,t) + \bar{\Gamma}_i(x,t)\tilde{z}_i(l(t),t) + \frac{c}{2}(\tilde{z}_i(x,t) + \tilde{w}_i(x,t))\\ &= \left(\sqrt{q}\bar{\phi}_i(x,x) + c\right)\tilde{\alpha}_i(x,t) + \int_x^{l(t)}\Bigg(\bar{\phi}_i(x,y)\frac{c}{2} - \sqrt{q}\bar{\phi}_{ix}(x,y) - \sqrt{q}\bar{\phi}_{iy}(x,y) - \frac{c}{2}\bar{\psi}_i(x,y)\\ &\quad - \bar{\phi}_i(x,y)\Bigg)\tilde{\alpha}_i(y,t)dy - \int_x^{l(t)}\Bigg(\int_x^y\bar{\phi}_i(x,z)\bar{M}_i(z,y)dz - \bar{M}_i(x,y) + \bar{\phi}_i(x,y)\frac{c}{2}\Bigg)\tilde{\beta}_i(y,t)dy + \Bigg(\bar{\Gamma}_i(x,t)\\ &\quad - \dot{l}(t)\bar{\phi}_i(x,l(t)) + \sqrt{q}\bar{\phi}_i(x,l(t))\Bigg)\tilde{\alpha}_i(l(t),t).\end{aligned} \tag{40}$$

Substituting the transformation (33)–(34) into (31), and inserting (36)–(37), through a lengthy calculation, we have

$$\begin{aligned}&\tilde{w}_{it}(x,t) - \sqrt{q}\tilde{w}_{ix}(x,t) + \Gamma_i(x,t)\tilde{z}_i(l(t),t) + \frac{c}{2}(\tilde{w}_i(x,t) + \tilde{z}_i(x,t))\\ &= \left(\frac{c}{2} - 2\sqrt{q}\bar{\psi}_i(x,x)\right)\tilde{\alpha}_i(x,t) + \int_x^{l(t)}\Bigg(-c\bar{\psi}_i(x,y) - \sqrt{q}\bar{\psi}_{iy}(x,y) + \sqrt{q}\bar{\psi}_{ix}(x,y) - \frac{c}{2}\bar{\phi}_i(x,y)\Bigg)\tilde{\alpha}_i(y,t)dy\\ &\quad + \int_x^{l(t)}\Bigg(\frac{c}{2}\bar{\psi}_i(x,y) + \bar{N}_i(x,y)\end{aligned}$$

$$-\int_x^y \bar{\psi}_i(x,z)\bar{M}_i(z,y)dz\Big)\tilde{\beta}_i(y,t)dy+\Big(\Gamma_i(x,t)$$
$$-\dot{l}(t)\bar{\psi}_i(x,l(t))+\sqrt{q}\bar{\psi}_i(x,l(t))\Big)\tilde{\alpha}_i(l(t),t). \tag{41}$$

To make sure the right hand sides of the equal signs in (40)–(41) are equal to zero, the kernels $\bar{\phi}_i(x,y)$, $\bar{\psi}_i(x,y)$ should satisfy

$$\Big(\frac{c}{2}-1\Big)\bar{\phi}_i(x,y)-\sqrt{q}\bar{\phi}_{ix}(x,y)-\sqrt{q}\bar{\phi}_{iy}(x,y)-\frac{c}{2}\bar{\psi}_i(x,y)=0, \tag{42}$$

$$-c\bar{\psi}_i(x,y)-\sqrt{q}\bar{\psi}_{iy}(x,y)+\sqrt{q}\bar{\psi}_{ix}(x,y)-\frac{c}{2}\bar{\phi}_i(x,y)=0, \tag{43}$$

$$\bar{\phi}_i(x,x)=-\frac{c}{\sqrt{q}}, \tag{44}$$

$$\bar{\psi}_i(x,x)=\frac{c}{4\sqrt{q}}. \tag{45}$$

$\bar{M}_i(x,y)$, $\bar{N}_i(x,y)$ in (36) and (37) satisfy

$$\bar{M}_i(x,y)=\frac{c}{2}\bar{\phi}_i(x,y)+\int_x^y \bar{\phi}_i(x,z)\bar{M}_i(z,y)dz, \tag{46}$$

$$\bar{N}_i(x,y)=-\frac{c}{2}\bar{\psi}_i(x,y)+\int_x^y \bar{\psi}_i(x,z)\bar{M}_i(z,y)dz. \tag{47}$$

The observer gains $\Gamma_i(x,t)$, $\bar{\Gamma}_i(x,t)$ are thus obtained as

$$\Gamma_i(x,t)=\dot{l}(t)\bar{\psi}_i(x,l(t))-\sqrt{q}\bar{\psi}_i(x,l(t)), \tag{48}$$

$$\bar{\Gamma}_i(x,t)=\dot{l}(t)\bar{\phi}_i(x,l(t))-\sqrt{q}\bar{\phi}_i(x,l(t)). \tag{49}$$

Lemma 1. *The kernel equations (42)–(45) have a unique continuous solution $(\bar{\psi}_i(x,y),\bar{\phi}_i(x,y))$ in $D_o=\{(x,y)|0\le x\le y\le l(t)\}$.*

The proof of Lemma 1 is shown in the Appendix.

3.4. Exponentially convergence of the observer error

After obtaining the observer gains $\bar{\Gamma}_i(x,t)$, $\Gamma_i(x,t)$, we prove the exponential stability of the observer error dynamics (29)–(32) with the designed $\bar{\Gamma}_i(x,t)$, $\Gamma_i(x,t)$ in the following lemma, the proof of which is shown in the Appendix.

Lemma 2. *If initial values $(\tilde{z}_i(x,t_0),\tilde{w}_i(x,t_0))\in L^2(0,L_0)$, the observer error system (29)–(32) is uniformly exponentially stable in the sense of the norm*

$$\Big(\sum_{i=1}^{2}\big(\|\tilde{z}_i(\cdot,t)\|^2+\|\tilde{w}_i(\cdot,t)\|^2\big)+\big|\tilde{X}(t)\big|^2\Big)^{\frac{1}{2}}, \tag{50}$$

where $L^2(0,L_0)$ is the usual Hilbert space with $L_0=l(t_0)$ being the initial length of the cable at the initial time t_0.

Using Lemma 2 and (28), it is straightforward to prove the following theorem.

Theorem 1. *If initial values $(z_i(x,t_0),w_i(x,t_0))\in L^2(0,L_0)$ and $(\hat{z}_i(x,t_0),\hat{w}_i(x,t_0))\in L^2(0,L_0)$, the observer (22)–(27) can track the system (15)–(19) with uniformly exponentially convergent errors in the sense of*

$$\sum_{i=1}^{2}\big(\|z_i(\cdot,t)-\hat{z}_i(\cdot,t)\|^2+\|w_i(\cdot,t)-\hat{w}_i(\cdot,t)\|^2\big)+\big|X(t)-\hat{X}(t)\big|^2. \tag{51}$$

Theorem 1 shows the proposed observer can recover the distributed states of the plant (15)–(19) only using the available boundary measurements. Moreover, the following lemma holds as well, the proof of which is shown in the Appendix.

Lemma 3. *For any initial data $(\tilde{z}_i(x,t_0),\tilde{w}_i(x,t_0))\in H^1(0,L_0)$, the observer error system (29)–(32) is uniformly exponentially stable in the sense of*

$$\sum_{i=1}^{2}\big(\|\tilde{z}_{ix}(\cdot,t)\|^2+\|\tilde{w}_{ix}(\cdot,t)\|^2\big)^{\frac{1}{2}}, \tag{52}$$

where $H^1(0,L_0)=\{u|u(\cdot,t)\in L^2(0,L_0),u_x(\cdot,t)\in L^2(0,L_0)\}$.

4. Output feedback controller design

In Section 3, we have built the observer which can exponentially track the distributed states of the system (15)–(19). In this section, we design output feedback control laws $U_1(t)$, $U_2(t)$ by using the states recovered from the observer via the backstepping method (Krstic, 2009; Krstic & Smyshlyaev, 2008).

4.1. Backstepping transformation and target system

The design of the observer-based output feedback controller is based on the observer (22)–(27). Using the backstepping transformation

$$\alpha_i(x,t)\equiv\hat{z}_i(x,t), \tag{53}$$

$$\beta_i(x,t)=\hat{w}_i(x,t)-\int_0^x\psi_i(x,y)\hat{z}_i(y,t)dy-\int_0^x\phi_i(x,y)\hat{w}_i(y,t)dy-\gamma_i(x)\hat{X}(t), \tag{54}$$

we would like to convert the observer system-$(\hat{z}_i,\hat{w}_i,\hat{X}(t))$ (22)–(27) to the following target system-$(\alpha_i,\beta_i,\hat{X}(t))$:

$$\dot{\hat{X}}(t)=\Big(\bar{A}+\sum_{i=1}^{2}B_i\kappa_i\Big)\hat{X}(t)+\sum_{i=1}^{2}\frac{B_i}{\sqrt{q}}\beta_i(0,t)+\bar{L}(C_1+C_2)\tilde{X}(t), \tag{55}$$

$$\alpha_{it}(x,t)=-\sqrt{q}\alpha_{ix}(x,t)-c\beta_i(x,t)-c\alpha_i(x,t)+c\int_0^x\psi_i^I(x,y)\alpha_i(y,t)dy+c\int_0^x\phi_i^I(x,y)\beta_i(y,t)dy+c\gamma_i^I(x)\hat{X}(t)+\bar{\Gamma}_i(x,t)\tilde{z}_i(l(t),t), \tag{56}$$

$$\beta_{it}(x,t)=\sqrt{q}\beta_{ix}(x,t)-\lambda_i(x)\beta_j(0,t)-\frac{c}{2}\beta_i(x,t)-\mathcal{N}(x,t)\tilde{z}_i(l(t),t)-\mathcal{N}_1(x)\tilde{X}(t), \tag{57}$$

$$\alpha_i(0,t)=\bar{D}_i\hat{X}(t)-\beta_i(0,t)+D_i\tilde{X}(t), \tag{58}$$

$$\beta_i(l(t),t)=0, \tag{59}$$

where

$$\mathcal{N}_i(x,t)=\int_0^x(\phi_i(x,y)\Gamma_i(y,t)+\psi_i(x,y)\bar{\Gamma}_i(y,t))dy+\Gamma_i(x,t), \tag{60}$$

$$\mathcal{N}_{1i}(x)=\gamma_i(x)\bar{L}(C_1+C_2)+\sqrt{q}\psi_i(x,0)D_i. \tag{61}$$

$\acute{A}=\bar{A}+\sum_{i=1}^{2}B_i\kappa_i$ is Hurwitz by choosing the row vectors κ_i because $(\bar{A},B_1+B_2)$ is controllable. $\bar{D}_1=D_1-\gamma_1(0)$ and $\bar{D}_2=D_2-\gamma_2(0)$.

$\lambda_i(x)$ is to be determined later. $\psi_i^I(x,y)$, $\phi_i^I(x,y)$, $\gamma_i^I(x)$ are kernels in the inverse transformations as

$$\hat{z}_i(x,t) \equiv \alpha_i(x,t), \tag{62}$$

$$\hat{w}_i(x,t) = \beta_i(x,t) - \int_0^x \psi_i^I(x,y)\alpha_i(y,t)dy - \int_0^x \phi_i^I(x,y)\beta_i(y,t)dy - \gamma_i^I(x)\hat{X}(t). \tag{63}$$

In the following section, the kernels $\psi_i(x,y)$, $\phi_i(x,y)$, $\gamma_i(x)$ would be determined by mapping the observer system-$(\hat{z}_i, \hat{w}_i, \hat{X}(t))$ (22)–(27) and the target system-$(\alpha_i, \beta_i, \hat{X}(t))$ (55)–(59) via the transformations (53)–(54). The proof of the existence of kernels $\psi_i^I(x,y)$, $\phi_i^I(x,y)$, $\gamma_i^I(x)$ please refer to Section 2.4 in Wang, Krstic, and Pi (2018) for detail.

4.2. Calculation of kernels

Substituting (53)–(54) into (57), we have

$$\begin{aligned}
&\beta_{it}(x,t) - \sqrt{q}\beta_{ix}(x,t) + \lambda_i(x)\beta_j(0,t) + \frac{c}{2}\beta_i(x,t) \\
&+ \mathcal{N}_i(x,t)\tilde{z}_i(l(t),t) + \mathcal{N}_{1i}(x)\tilde{X}(t) \\
&= \left(-\frac{c}{2} + 2\sqrt{q}\psi_i(x,x)\right)\hat{z}_i(x,t) \\
&\quad + \int_0^x \left(\frac{c}{2}\psi_i(x,y) + \sqrt{q}\phi_{ix}(x,y) + \sqrt{q}\phi_{iy}(x,y)\right)\hat{w}_i(y,t)dy \\
&\quad + \int_0^x \left(\frac{c}{2}\phi_i(x,y) + \sqrt{q}\psi_{ix}(x,y) - \sqrt{q}\psi_{iy}(x,y)\right)\hat{z}_i(y,t)dy \\
&\quad + \left(\sqrt{q}\gamma_i'(x) - \gamma_i(x)(\bar{A} + \frac{c}{2}) \right. \\
&\quad \left. - 2\psi_i(x,0)D_i + \frac{1}{\sqrt{q}}\gamma_i(x)B_j\gamma_j(0)\right)\hat{X}(t) \\
&\quad + \left(\sqrt{q}\phi_i(x,0) - \gamma_i(x)B_i\frac{1}{\sqrt{q}} + \psi_i(x,0)\right)\hat{w}_i(0,t) \\
&\quad + \left(\lambda_i(x) - \frac{1}{\sqrt{q}}\gamma_i(x)B_j\right)\hat{w}_j(0,t).
\end{aligned} \tag{64}$$

To guarantee the right hand side of the equal sign in (64) are equal to zero, which ensures (57), and mapping the ODEs (22), (55), we have the following kernel conditions:

$$\frac{c}{2}\psi_i(x,y) + \sqrt{q}\phi_{ix}(x,y) + \sqrt{q}\phi_{iy}(x,y) = 0, \tag{65}$$

$$\frac{c}{2}\phi_i(x,y) + \sqrt{q}\psi_{ix}(x,y) - \sqrt{q}\psi_{iy}(x,y) = 0, \tag{66}$$

$$\sqrt{q}\phi_i(x,0) - \frac{1}{\sqrt{q}}\gamma_i(x)B_i + \psi_i(x,0) = 0, \tag{67}$$

$$\psi_i(x,x) = \frac{c}{4\sqrt{q}}, \tag{68}$$

$$\gamma_i'(x) - \frac{1}{\sqrt{q}}\gamma_i(x)\left(\bar{A} + \frac{c}{2} - \frac{1}{\sqrt{q}}B_j\gamma_j(0)\right) - \frac{2}{\sqrt{q}}\psi_i(x,0)D_i = 0, \tag{69}$$

$$\gamma_i(0) = \sqrt{q}\kappa_i, \tag{70}$$

$$\lambda_i(x) - \frac{1}{\sqrt{q}}\gamma_i(x)B_j = 0. \tag{71}$$

The following lemma shows that there exists a unique continuous solution $(\psi_i(x,y), \phi_i(x,y), \gamma_i(x,t))$ of (65)–(70). The proof is shown in the Appendix.

Lemma 4. *The kernel equations (65)–(70) have a unique continuous solution $(\psi_i(x,y), \phi_i(x,y), \gamma_i(x))$ in $D = \{(x,y)|0 \le y \le x \le l(t)\}$.*

$\lambda_i(x)$ is then obtained through (71). Using the obtained kernels, we then would derive the control law in the following section.

Note that (56) and (58) are obtained by substituting (62)–(63) into (23), (25)–(26) straightforward.

4.3. Control law and realization

Considering the boundary condition (59) in the target system, the boundary condition (27) in the observer, and the transformation (54), we derive the controller as:

$$\begin{aligned}
U_{e1}(t) = \frac{-1}{2\sqrt{q}}\Bigg(&z_1(l(t),t) - \int_0^{l(t)}\psi_1(l(t),y)\hat{z}_1(y,t)dy \\
&- \int_0^{l(t)}\phi_1(l(t),y)\hat{w}_1(y,t)dy - \gamma_1(l(t))\hat{X}(t)\Bigg),
\end{aligned} \tag{72}$$

$$\begin{aligned}
U_{e2}(t) = \frac{-1}{2\sqrt{q}}\Bigg(&z_2(l(t),t) - \int_0^{l(t)}\psi_2(l(t),y)\hat{z}_2(y,t)dy \\
&- \int_0^{l(t)}\phi_2(l(t),y)\hat{w}_2(y,t)dy - \gamma_2(l(t))\hat{X}(t)\Bigg).
\end{aligned} \tag{73}$$

The signals $\hat{z}_i(x,t)$, $\hat{w}_i(x,t)$, $\hat{X}(t)$ are obtained from the observer (22)–(27) constructed by measurements $\ddot{y}(t)$, $\ddot{\theta}(t)$ and $u_x(l(t),t)$, $v_x(l(t),t)$, $u_t(l(t),t)$, $v_t(l(t),t)$ which are also used to calculate $z_i(l(t),t)$. The gains $(\psi_i(x,y), \phi_i(x,y), \gamma_i(x))$ are the solution of (65)–(70).

Using (72)–(73), the two control inputs $U_1(t)$ and $U_2(t)$ of (1)–(6) are derived as

$$U_1(t) = U_{e1}(t) - U_{e2}(t),\ U_2(t) = U_{e1}(t) + U_{e2}(t). \tag{74}$$

Realization of the proposed controller:

- All signals required in the controller are available measurements in the mining cable elevator.
- The highest time derivative signals used in the controller are first-order derivatives $u_t(l(t),t)$, $v_t(l(t),t)$, $\dot{y}(t)$, $\dot{\theta}(t)$. Physically, they are velocities and are measurable or easily deducible from acceleration measurements.
- The closed-loop system has the robustness with respect to the time-delay in the feedback loop, because the gain γ (Logemann, Rebarber, & Weiss, 1996) of the open-loop transfer function can be proved as $\gamma < 1$ when $s \to \infty$. The proof is omitted here due to the space limit.
- If unknown disturbances are considered at the boundaries, the disturbance estimation and attenuation techniques (Wang, Tang, Pi, & Krstic, 2017; Wang, Tang et al., 2018) in wave PDE modeled mining cable elevators can be incorporated into the design.

4.4. Stability of the system-$(\hat{z}_i, \hat{w}_i)$

The following lemma would show the exponential stability of the system-$(\hat{z}_i, \hat{w}_i)$ (22)–(27) under the control (72)–(73). The proof is shown in the Appendix.

Lemma 5. *If initial values $(\hat{z}_i(x,t_0), \hat{w}_i(x,t_0)) \in L^2(0,L_0)$, the system $(\hat{z}_i(x,t), \hat{w}_i(x,t))$ (22)–(27) under the control law (72)–(73) is uniformly exponentially stable in the sense of the norm*

$$\left(\sum_{i=1}^{2}\left(\|\hat{z}_i(\cdot,t)\|^2 + \|\hat{w}_i(\cdot,t)\|^2\right) + \left|\hat{X}(t)\right|^2\right)^{1/2}. \tag{75}$$

Based on the exponential stability result of the system-$(\hat{z}_i, \hat{w}_i, \hat{X})$ in the sense of $\|\hat{z}_i(\cdot,t)\|^2 + \|\hat{w}_i(\cdot,t)\|^2 + |\hat{X}(t)|^2$, we can obtain the exponential stability estimate in the sense of $\|\hat{z}_{ix}(\cdot,t)\|^2 + \|\hat{w}_{ix}(\cdot,t)\|^2$ in the following lemma, the proof of which is shown in the Appendix.

Lemma 6. *For any initial data* $(\hat{z}_i(x,t_0),\hat{w}_i(x,t_0)) \in H^1(0,L_0)$, *the system* (22)–(27) *under the control law* (72)–(73) *is uniformly exponentially stable in the sense of*

$$\sum_{i=1}^{2}\left(\|\hat{z}_{ix}(\cdot,t)\|^2+\|\hat{w}_{ix}(\cdot,t)\|^2\right)^{\frac{1}{2}}. \tag{76}$$

5. Stability under output feedback

The following theorems are used to show the achievement of the control objects proposed in Section 2 under the proposed output feedback controller which is bounded and exponentially convergent to zero.

Theorem 2. *If initial values* $(\hat{z}_i(x,t_0),\ \hat{w}_i(x,t_0),\ z_i(x,t_0),\ w_i(x,t_0)) \in H^1(0,L_0)$, *the closed-loop system including the plant* (15)–(19), *the controller* (72)–(73) *and the observer* (22)–(27) *has the following properties:*

(1) *The closed-loop system is uniformly exponentially stable in the sense of the norm:*

$$\begin{aligned}&\Big(\sum_{i=1}^{2}\big(\|\hat{z}_i(\cdot,t)\|^2+\|\hat{w}_i(\cdot,t)\|^2+\|z_i(\cdot,t)\|^2+\|w_i(\cdot,t)\|^2\\&+\|\hat{z}_{ix}(\cdot,t)\|^2+\|\hat{w}_{ix}(\cdot,t)\|^2+\|z_{ix}(\cdot,t)\|^2+\|w_{ix}(\cdot,t)\|^2\big)\\&+\left|\hat{X}(t)\right|^2+|X(t)|^2\Big)^{1/2},\end{aligned} \tag{77}$$

with a decay rate σ_{all} *which can be adjusted by the choices of the control parameters* κ_i, $\bar{L}$.

(2) *In the closed-loop system, there exist positive constants* σ_{Ui} *and* Υ_{0i} *making* $U_{e1}(t)$, $U_{e2}(t)$ *bounded and exponentially convergent to zero in the sense of*

$$|U_{e1}(t)|\le\Upsilon_{01}e^{-\sigma_{U1}t},\ |U_{e2}(t)|\le\Upsilon_{02}e^{-\sigma_{U2}t}. \tag{78}$$

Proof of (1). Recalling the exponential stability result in the sense of $\|\hat{z}_1(\cdot,t)\|^2+\|\hat{w}_1(\cdot,t)\|^2+\|\hat{z}_2(\cdot,t)\|^2+\|\hat{w}_2(\cdot,t)\|^2+|\hat{X}(t)|^2$ proved in Lemma 5 with the decay rate σ, and the exponential stability result in the sense of $\|\tilde{z}_1(\cdot,t)\|^2+\|\tilde{w}_1(\cdot,t)\|^2+\|\tilde{z}_2(\cdot,t)\|^2+\|\tilde{w}_2(\cdot,t)\|^2+|\tilde{X}(t)|^2$ proved in Lemma 2 with the decay rate σ_e, we obtain the exponential stability result in the sense of $\|z_1(\cdot,t)\|^2+\|w_1(\cdot,t)\|^2+\|z_2(\cdot,t)\|^2+\|w_2(\cdot,t)\|^2+|X(t)|^2$ via (28) with the decay rate $\sigma_o=\min\{\sigma,\sigma_e\}$.

Similarly, recalling the exponential stability estimate in the sense of $\|\hat{z}_{1x}(\cdot,t)\|^2+\|\hat{w}_{1x}(\cdot,t)\|^2+\|\hat{z}_{2x}(\cdot,t)\|^2+\|\hat{w}_{2x}(\cdot,t)\|^2$ proved in Lemma 6 with the decay rate σ_f, and the exponential stability estimate in the sense of $\|\tilde{z}_{1x}(\cdot,t)\|^2+\|\tilde{w}_{1x}(\cdot,t)\|^2+\|\tilde{z}_{2x}(\cdot,t)\|^2+\|\tilde{w}_{2x}(\cdot,t)\|^2$ proved in Lemma 3 with the decay rate σ_{eHf}, we obtain the exponential stability estimate in the sense of $\|z_{1x}(\cdot,t)\|^2+\|w_{1x}(\cdot,t)\|^2+\|z_{2x}(\cdot,t)\|^2+\|w_{2x}(\cdot,t)\|^2$ with the decay rate $\sigma_{oH}=\min\{\sigma_f,\sigma_{eHf}\}$.

Considering (120), (95), (136), (109), we know

$$\begin{aligned}\sigma_{all}&=\min\{\sigma_o,\sigma_{oH}\}=\min\{\sigma,\sigma_e,\sigma_f,\sigma_{eHf}\}\\&=\min\{\sigma,\sigma_e,\sigma_H,\sigma_{eH}\}\end{aligned} \tag{79}$$

can be adjusted by control parameters κ_i and $\bar{L}$. The proof of Property (1) in Theorem 2 is completed.

Proof of (2). Applying Cauchy–Schwarz inequality into (72)–(73), we have

$$\begin{aligned}&|U_{e1}(t)|^2+|U_{e2}(t)|^2\\&\le\sum_{i=1}^{2}\Big(\frac{1}{q}z_i(l(t),t)^2-\frac{1}{q}M_{10i}L\|\hat{z}_i(\cdot,t)\|^2\\&-\frac{1}{q}M_{11i}L\|\hat{w}_i(\cdot,t)\|^2-\frac{1}{q}M_{12i}\left|\hat{X}(t)\right|^2\Big),\end{aligned} \tag{80}$$

where $M_{10i}=\max\{\psi_i(l(t),y)^2\}$, $M_{11i}=\max\{\phi_i(l(t),y)^2\}$, $M_{12i}=\max\{\gamma_i(l(t))^2\}$ for $0<y<l(t)<L$ with L being the total length of the cables.

Using Cauchy–Schwarz inequality and (59), we have

$$\begin{aligned}|\beta_i(0,t)|^2&\le|\beta_i(l(t),t)|^2+\left|\int_0^{l(t)}\beta_{ix}(x,t)dx\right|^2\\&\le L\|\beta_{ix}(\cdot,t)\|^2.\end{aligned} \tag{81}$$

According to the exponential stability estimate in the sense of $\|\beta_{ix}(\cdot,t)\|^2$ in the proof of Lemma 6, we have $\beta_i(0,t)$ is exponentially convergent to zero. Recalling (54) at $x=0$ and the exponential convergence of $\hat{X}(t)$ proved in Lemma 5, we obtain that $\hat{w}_i(0,t)$ is exponentially convergent to zero. Recalling relationships (25)–(26) and the exponential convergence of $X(t)$ proved in Property (1), we obtain the exponential convergence of $\hat{z}_i(0,t)$.

Similarly, using Cauchy–Schwarz inequality and (39), recalling the exponential stability estimate in the sense of $\|\tilde{\beta}_{ix}(\cdot,t)\|^2$ in the proof of Lemma 3, we have $\tilde{\beta}_i(0,t)$ is exponentially convergent to zero, followed by which we obtain the exponential convergence of $\tilde{w}_i(0,t)$ via (34) at $x=0$. Together with the exponential convergence of $\hat{w}_i(0,t)$ proved above, we have that $w_i(0,t)$ is exponentially convergent to zero. Through (18), together with the exponential convergence of $X(t)$, we have $z_i(0,t)$ is exponentially convergent to zero as well. Using Cauchy–Schwarz inequality, we also have

$$\begin{aligned}|z_i(l(t),t)|^2&\le|z_i(0,t)|^2+\left|\int_0^{l(t)}z_{ix}(x,t)dx\right|^2\\&\le|z_i(0,t)|^2+L\|z_{ix}(\cdot,t)\|^2.\end{aligned} \tag{82}$$

We then obtain that $z_i(l(t),t)$ is exponentially convergent to zero when $t\to\infty$ by recalling the exponential stability estimate in the sense of $\|z_{ix}(\cdot,t)\|^2$ proved in Property (1) and the exponential convergence of $z_i(0,t)$ proved above. Together with the exponential stability in the sense of $\|\hat{z}_1(\cdot,t)\|^2+\|\hat{w}_1(\cdot,t)\|^2+\|\hat{z}_2(\cdot,t)\|^2+\|\hat{w}_2(\cdot,t)\|^2+|\hat{X}(t)|^2$ proved in Lemma 5, we obtain that control inputs $U_{e1}(t)$, $U_{e2}(t)$ are bounded and exponentially convergent to zero. The proof of Property (2) in Theorem 2 is completed.

According to Theorem 2, we can obtain the stability properties of the systems (u,v) and (e,s) in the following theorem.

Theorem 3. *If initial values* $(u(x,t_0),v(x,t_0))\in H^2(0,L_0)$, $(e(x,t_0),s(x,t_0))\in H^2(0,L_0)$, *the original closed-loop system-*(u,v) *including the plant* (1)–(6) *with the controllers* (74) *is uniformly exponentially stable in the sense of*

$$\begin{aligned}&\|u_t(\cdot,t)\|+\|u_x(\cdot,t)\|+\|v_t(\cdot,t)\|+\|v_x(\cdot,t)\|+\|u_{xt}(\cdot,t)\|\\&+\|u_{xx}(\cdot,t)\|+\|v_{xt}(\cdot,t)\|+\|v_{xx}(\cdot,t)\|,\end{aligned} \tag{83}$$

where $H^2(0,L_0)=\{u|u(\cdot,t)\in L^2(0,L_0),u_x(\cdot,t)\in L^2(0,L_0),u_{xx}(\cdot,t)\in L^2(0,L_0)\}$. *The system-*$(e,s)$ *obtained from* (9)–(10) *is also uniformly exponentially stable in the sense of*

$$\begin{aligned}&\|e_t(\cdot,t)\|+\|e_x(\cdot,t)\|+\|s_t(\cdot,t)\|+\|s_x(\cdot,t)\|+\|e_{xt}(\cdot,t)\|\\&+\|e_{xx}(\cdot,t)\|+\|s_{xt}(\cdot,t)\|+\|s_{xx}(\cdot,t)\|.\end{aligned} \tag{84}$$

The exponential decay rates can be adjusted by the control parameters κ_i, $\bar{L}$. *Moreover, the controllers* $U_1(t)$, $U_2(t)$ *realized by hydraulic actuators at the floating sheaves are bounded and exponentially convergent to zero.*

Proof. Considering (11)–(14), applying Cauchy–Schwarz inequality, we obtain

$$\|e_t(\cdot,t)\|^2 \le \frac{1}{2}\|z_i(\cdot,t)\|^2 + \frac{1}{2}\|w_i(\cdot,t)\|^2, \tag{85}$$

$$\|e_x(\cdot,t)\|^2 \le \frac{1}{2q}\|w_i(\cdot,t)\|^2 + \frac{1}{2q}\|z_i(\cdot,t)\|^2, \tag{86}$$

$$\|e_{xt}(\cdot,t)\|^2 \le \frac{1}{2}\|z_{ix}(\cdot,t)\|^2 + \frac{1}{2}\|w_{ix}(\cdot,t)\|^2, \tag{87}$$

$$\|e_{xx}(\cdot,t)\|^2 \le \frac{1}{2q}\|w_{ix}(\cdot,t)\|^2 + \frac{1}{2q}\|z_{ix}(\cdot,t)\|^2 \tag{88}$$

for $i = 2$, and $\|s_t(\cdot,t)\|^2$, $\|s_x(\cdot,t)\|^2$, $\|s_{xt}(\cdot,t)\|^2$, $\|s_{xx}(\cdot,t)\|^2$ have the same inequality relationships with (85)–(88) for $i = 1$. Therefore, recalling the exponential stability with the decay rate σ_{all} in the sense of $\|z_i(\cdot,t)\|^2 + \|w_i(\cdot,t)\|^2 + \|z_{ix}(\cdot,t)\|^2 + \|w_{ix}(\cdot,t)\|^2$ proved in Property (1) in Theorem 2, we obtain that the system-(e, s) obtained from (9)–(10) is exponentially stable in the sense of (84) with the decay rate at least σ_{all}.

According to the definition (9)–(10), it is then straightforward to obtain that the system (1)–(6) is exponentially stable in the sense of (83) with the decay rate at least σ_{all} which can be adjusted by the control parameters κ_i, $\bar{L}$.

Recalling (74) and Property (2) in Theorem 2, we obtain the controller $U_1(t)$, $U_2(t)$ at the floating sheaves are bounded and exponentially convergent to zero. The proof of Theorem 3 is completed.

According to the exponential convergence of $X(t)$ proved in Property (1) of Theorem 2 and the exponential stability estimate in the sense of the norms including $\|u_{xx}(\cdot,t)\| + \|v_{xx}(\cdot,t)\|$ and $\|e_{xx}(\cdot,t)\| + \|s_{xx}(\cdot,t)\|$ proved in Theorem 3, with the adjustable exponential decay rates, we can state that the control objectives proposed in Section 2 are achieved.

6. Simulation

The physical parameters of the mining cable elevator (1)–(6) used in the simulation are shown in Table 1. The designed reference of the hoisting velocity $\dot{l}(t)$ is plotted in Fig. 3. The control parameters chosen here are $\bar{L} = [1, 1, 1, 1]^T$, $\kappa_1 = [0.0016, 0, 0.03, 0]^T$ and $\kappa_2 = [0, -0.0018, 0, -0.03]^T$.

We also apply the boundary damper which is classically utilized in industries at the head sheaves to compare with the proposed output feedback controller. The boundary dampers:

$$\begin{aligned} U_{d1}(t) &= k_{d1}\dot{u}(l(t),t) = k_{d1}(u_t(l(t),t) + \dot{l}(t)u_x(l(t),t)) \\ &= k_{d1}\Big(\frac{1}{4}(z_1(l(t),t) + w_1(l(t),t) - z_2(l(t),t) - w_2(l(t),t)) \\ &\quad + \frac{\dot{l}(t)}{4\sqrt{q}}((w_1(l(t),t) - z_1(l(t),t)) \\ &\quad - (w_2(l(t),t) - z_2(l(t),t)))\Big), \end{aligned} \tag{89}$$

$$\begin{aligned} U_{d2}(t) &= k_{d2}\dot{v}(l(t),t) = k_{d2}(v_t(l(t),t) + \dot{l}(t)v_x(l(t),t)) \\ &= k_{d2}\Big(\frac{1}{4}(z_1(l(t),t) + w_1(l(t),t) + z_2(l(t),t) + w_2(l(t),t)) \\ &\quad + \frac{\dot{l}(t)}{4\sqrt{q}}((w_1(l(t),t) - z_1(l(t),t)) \\ &\quad + (w_2(l(t),t) - z_2(l(t),t)))\Big), \end{aligned} \tag{90}$$

where k_{d1}, k_{d2} are tuned to attain the efficient control performance. We have tested different values of k_{d1}, k_{d2}, and the best regulating performance is achieved with $k_{d1} = -0.33$, $k_{d2} = -0.31$.

Table 1
Physical parameters of the dual-cable mining elevator.

Parameters (units)	Values
Initial length L (m)	2000
Final length (m)	50
Cable effective steel area A_a (m^2)	0.47×10^{-3}
Cable effective Youngs modulus E (N/m^2)	2.1×10^{10}
Cable linear density ρ (kg/m)	8. 1
Total hoisted mass M (kg)	15 000
Moment of inertia of the cage J_c ($kg{\cdot}m^2$)	17 500
Gravitational acceleration g (m/s^2)	9.8
Maximum hoisting velocities $\bar{v}_{\max}$ (m/s)	16.25
Total hoisting time t_f (s)	150
Cable material damping coefficient $\bar{c}$ (N·s/m)	0.6
Cage axial damping coefficient c_d (N·s/m)	0.4
Cage roll damping coefficient c_a (N·m·s/rad)	0.4
Cage dimension l_1 (m)	2.5
Cage dimension l_r (m)	3.53
Cage dimension φ (rad)	0.785

Cage dimensions referred to Fig. 1.

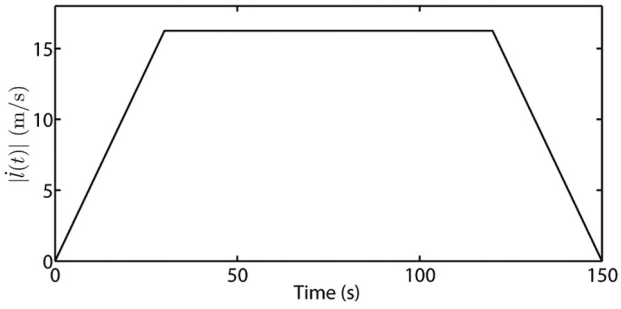

Fig. 3. The hoisting velocity $\dot{l}(t)$.

6.1. Calculation method

The simulation is performed for the physical model-(z_1, w_1, z_2, w_2, X) (15)–(19) with the control law (72)–(73) and the observer (22)–(27). The responses of tension oscillations $E_A u_x(x,t)$, $E_A v_x(x,t)$ in the cables can be calculated by those of z_1, w_1, z_2, w_2 through (11)–(14) and (9)–(10). The actual control forces $E_A U_1(t)$, $E_A U_2(t)$ applied at the two floating head sheaves are obtained via (74).

The simulation is performed by the finite-difference method for the discretization in time and space after converting the time-varying domain PDE to a fixed domain PDE via introducing $\check{\xi} = \frac{x}{l(t)}$ (Wang, Pi et al., 2017), and the time step and space step are chosen as 0.001 and 0.05 respectively. The solutions of the kernel equations (42)–(45) and (65)–(70) which are coupled linear hyperbolic PDEs are also solved by the finite difference method.

6.2. Initial conditions

The initial conditions of the plant (1)–(6) are obtained from the physical conditions of the dual-cable mining elevator with initial unbalance. In detail, the initial profiles of the axial strain $u_x(x,0)$, $v_x(x,0)$ are obtained by the force balance equations at the static state, which are written as

$$u_x(x,0) = \frac{\rho x g + M_{e1} g}{E_A},\ v_x(x,0) = \frac{\rho x g + M_{e2} g}{E_A}, \tag{91}$$

where M_{e1} and M_{e2} are loads at the bottoms of the two cables. Define the loads M_{e1}, M_{e2} are 9250 kg and 5750 kg. The difference between the loads supported by two cables might come from the imprecision of manufacture and installation of the two cables, or eccentricity of cage which always happens in loading, which

results to the initial strain error of the two cables according to (91). Note that this initial strain error of the plant is unknown in the control system design. The initial vibration velocities of two cables are defined as $u_t(x,0) = 0$, $v_t(x,0) = 0$, because the initial vibration velocity of each point in the cable is zero. The initial condition of $X(t)$ is defined as $X(0) = [y(0), \theta(0), \dot{y}(0), \dot{\theta}(0)]^T = [0,0,0,0]^T$.

After obtaining the initial conditions of $u_t(x,0)$, $v_t(x,0)$, $u_x(x,0)$, $v_x(x,0)$, according to (11)–(14) and (9)–(10), the initial conditions $(z_i(x,0), w_i(x,0))$ of (15)–(19) tested in simulation can be obtained. Similarly, the initial conditions $\hat{z}_i(x,0)$, $\hat{w}_i(x,0)$ of the observer (22)–(27) are defined. Please note that $M_{e1} = M_{e2} = M/2$ is used in (91) to obtain $u_x(x,0)$, $v_x(x,0)$ used to define the observer initial conditions, because the initial error between loads M_{e1}, M_{e2} is unknown in the observer design. Thus parts of the observer initial conditions are equal to those of the plant initial conditions as $\hat{z}_1(x,0) = z_1(x,0)$, $\hat{w}_1(x,0) = w_1(x,0)$, and the others are different from the plant initial conditions as $\hat{z}_2(x,0) \neq z_2(x,0)$, $\hat{w}_2(x,0) \neq w_2(x,0)$.

6.3. Results

Tension oscillations in cables: The tension oscillation is an important physical variable to investigate the strength of the cable. The suppression of tension oscillations is beneficial for easing the fatigue damage and prolonging the service life of the hoisting cables in the mining elevator. The responses of tension oscillations at the midpoint of cable 1 and cable 2 are shown in Figs. 4 and 5 respectively, with the open-loop, the boundary damper, and the proposed control law. The red dashed line, open loop response, in Figs. 4 and 5 show that the large tension oscillations would be caused obviously in the accelerated ascending process considering the hoisting velocity curve $\dot{l}(t)$ in Fig. 2. To suppress the oscillations of tension, the proposed output feedback controller and the boundary damper are applied at the head sheaves respectively and the responses are shown in black and blue lines in Figs. 4 and 5. It can be seen that tension oscillations are suppressed by both the proposed control law and the boundary damper. Moreover, we can observe that the responses with the proposed control law have faster convergence and less overshoot than the responses with the boundary damper.

Error of tension oscillations between cables: Error of tension oscillations between cables is also an important physical index to investigate the fatigue damage and prolonging the service life of the cables in dual-cable mining elevators. Because the constant mass of the cage are carried by two cables, the larger tension oscillation error between cables means the larger maximum load would be supported by one of the cables, the service life of which would be shorten due to the more serious fatigue damage. The errors between cables under the open-loop, the boundary damper, and the proposed control law are shown in Fig. 6. It shows that the tension oscillation error increases in 0–30 s which is the accelerated ascending process in the open-loop case, while it is reduced and convergent to zero under the proposed output feedback controller, moreover, with a faster convergence than the boundary damper.

Axial and roll vibrations of the cage: Axial and roll vibrations of the cage not only would bring uncomfortable feeling to passengers, but also would increase the tension error between two cables which would cause overburdened load for one of cables and result to fatigue fracture. The responses of the axial and roll vibrations of the cage are shown in Figs. 7–8 in the cases of without control, with the boundary damper, and with the proposed output feedback controller. It can be observed that the large axial vibrations and roll of the cage in open loop are suppressed to zero more efficiently

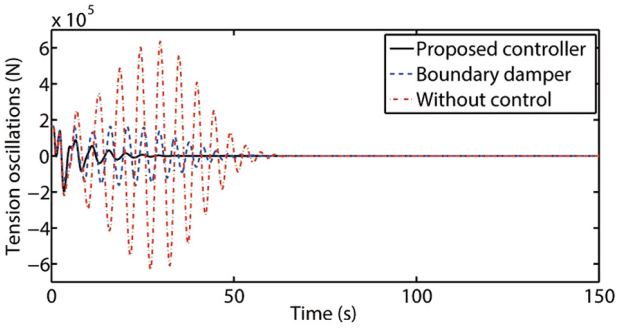

Fig. 4. Tension oscillations $E_A \times u_x(l(t)/2, t)$ at the midpoint of cable 1.

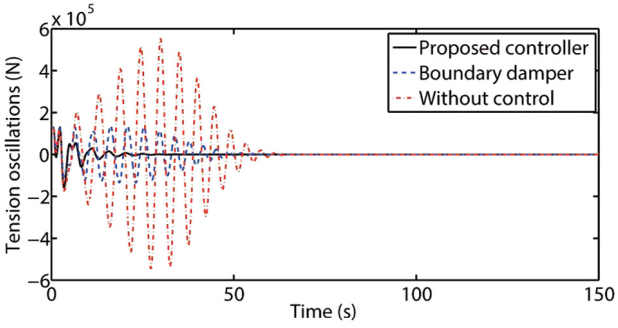

Fig. 5. Tension oscillations $E_A \times v_x(l(t)/2, t)$ at the midpoint of cable 2.

under the proposed output feedback controller than the traditional boundary damper, with the faster convergence and less overshoot.

Observer errors and output feedback control forces: The states used in the output feedback control forces (72)–(73) are the states recovered from the observer (22)–(27). Fig. 9 shows the convergent observer errors between $\hat{z}_2$, $\hat{w}_2$ and the plant states z_2, w_2 at the midpoint of the domain $[0, l(t)]$, which reflects the observer (22)–(27) can reconstruct their actual distributed states in (15)–(19), because the locations of the actuator and the sensors are at the boundaries, the estimation of the states at the midpoint $x = l(t)/2$ is the most challenging due to its accessibility. Note that the initial conditions of the observer $\hat{z}_1(x,0)$, $\hat{w}_1(x,0)$ are the same as those of the plant $z_1(x,0)$, $w_1(x,0)$, the observer errors of z_1, w_1 are thus at a very small magnitude 10^{-14} and convergent to zero as well. We only show the observer errors of z_2, w_2 here due to the space limit. The control forces $E_A U_1(t)$, $E_A U_2(t)$ obtained from (72)–(73) with (74) at the two head sheaves in the closed-loop system are given in Fig. 10, which shows the control forces $E_A U_1(t)$, $E_A U_2(t)$ are bounded and convergent to zero.

7. Conclusion and future work

In this paper, we proposed observer-based output feedback control laws using the available boundary measurements applied at the two floating head sheaves of the dual-cable mining elevator, to suppress the tension oscillations in each cable, the error of the tension oscillations between two cables and the axial and roll vibrations of the cage. Mathematically, the boundary observer-based output feedback control laws are designed to exponentially stabilize a system consisting of two pairs of 2×2 heterodirectional coupled hyperbolic PDEs on a time-varying domain and all four PDE bottom boundaries coupled at one ODE. The H^1 uniform exponential stability of the closed-loop system including the proposed output-feedback controller and the observer has been proved by

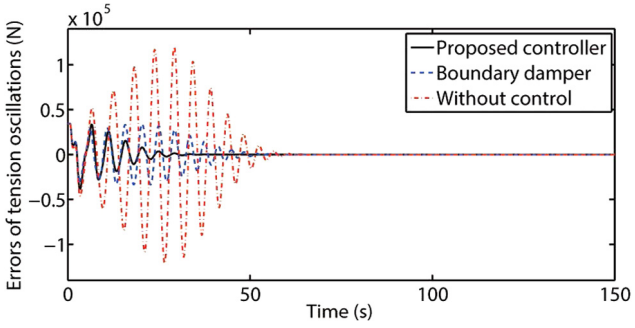

Fig. 6. Errors $E_A \times (u_x(l(t)/2, t) - v_x(l(t)/2, t))$ of tension oscillations between cable 1 and cable 2.

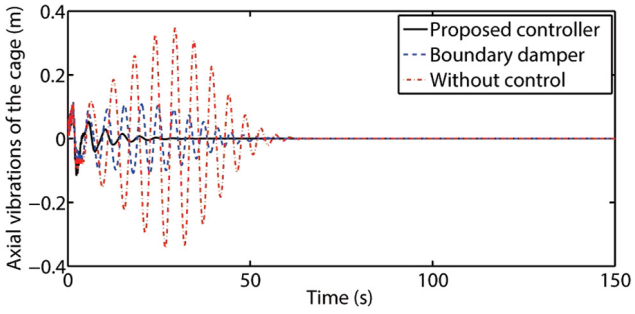

Fig. 7. Axial vibration displacements $y(t)$ of the cage.

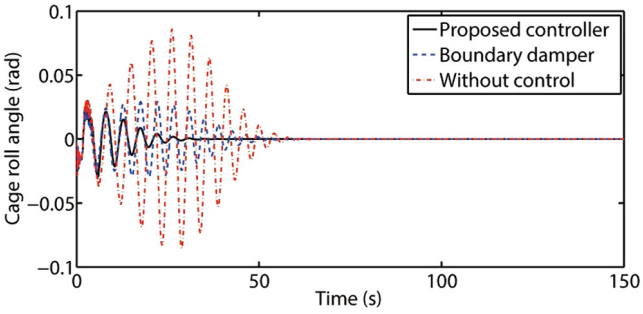

Fig. 8. Cage roll angles $\theta(t)$.

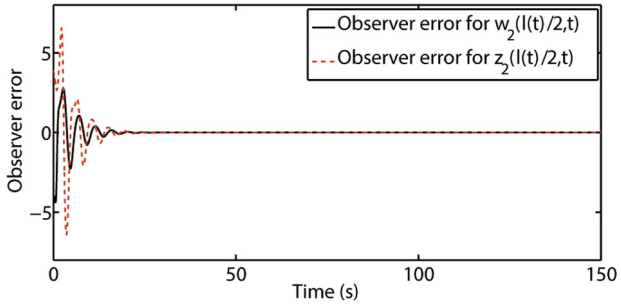

Fig. 9. Observer errors $z_2(l(t)/2, t) - \hat{z}_2(l(t)/2, t)$ and $w_2(l(t)/2, t) - \hat{w}_2(l(t)/2, t)$ between the plant (15)–(19) and the observer (22)–(27).

Lyapunov analysis. The simulation results illustrate the effective performance of the proposed control law.

In future work, the effect of the vibration states $u(x, t)$, $v(x, t)$ on the motion state $l(t)$ will be considered in a more accurate model which would be a nonlinear PDE with a state-depended

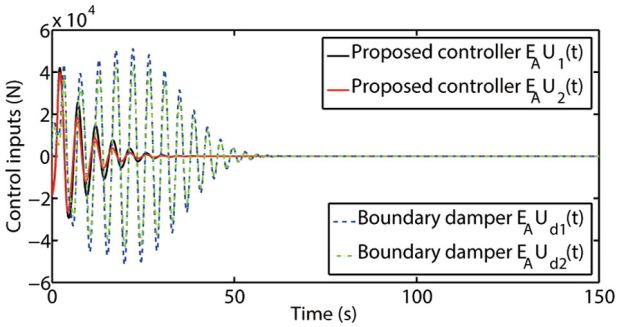

Fig. 10. The proposed observer-based output feedback control forces $E_A U_1(t) = E_A(U_{e2} + U_{e1})$, $E_A U_2(t) = E_A(U_{e2} - U_{e1})$ and the boundary dampers (89)–(90) at two head sheaves.

varying domain. The motion control force $U_a(t)$ for $l(t)$ and the vibration/tension control force $U_i(t)$ for $u(x, t)$, $v(x, t)$ will be designed synchronously.

Appendix

Proof of Lemma 1. The kernel equations (42)–(45) have the same form as the kernel equations (29)–(33) in Hu et al. (2016). In detail, (42) and (43) are two coupled transport PDEs with boundary conditions (44) and (45), which are the same form as the two coupled transport PDEs (32), (33) with boundary conditions (29), (30) in Hu et al. (2016) through setting $m = n = 1$ and replacing the K, L as $\bar{\phi}_i$, $\bar{\psi}_i$. The kernel equations of (29)–(33) have been proved well-posed in Hu et al. (2016). Under the boundedness and enough regularity assumptions (Assumptions 1 and 2) on the time-varying domain $l(t)$, Lemma 1 can then be proved.

Proof of Lemma 2. First, we establish the stability proof of the target system-$(\tilde{\alpha}_1, \tilde{\beta}_1, \tilde{\alpha}_2, \tilde{\beta}_2, \tilde{X})$. (35)–(39) which is a PDE-ODE cascaded system, where the states of the PDE subsystem $(\tilde{\alpha}_i, \tilde{\beta}_i)$ (36)–(39) which has a same structure as the exponentially stable target system (17)–(20) in Bin and Di Meglio (2017) flow into the ODE (35) with a Hurwitz state matrix $\hat{A}$. Therefore, the target system would be exponentially stable. Through the following Lyapunov analysis, we know the exponential decay rate can be adjusted by the control parameters. The Lyapunov function V_e for the system-$(\tilde{\alpha}_1, \tilde{\beta}_1, \tilde{\alpha}_2, \tilde{\beta}_2, \tilde{X})$ is defined as

$$V_e(t) = \sum_{i=1}^{2} V_{ei}(t), \tag{92}$$

where,

$$V_{ei}(t) = \tilde{X}^T(t) P_2 \tilde{X}(t) + \frac{\bar{a}_i}{2} \int_0^{l(t)} e^{\bar{\delta}_{2i} x} \tilde{\beta}_i(x, t)^2 dx + \frac{\bar{b}_i}{2} \int_0^{l(t)} e^{-\bar{\delta}_{1i} x} \tilde{\alpha}_i(x, t)^2 dx, \tag{93}$$

where the matrix $P_2 = P_2^T > 0$ is the solution to the Lyapunov equation $P_2 \hat{A} + \hat{A}^T P_2 = -Q_2$, for some $Q_2 = Q_2{}^T > 0$. The positive parameters $\bar{a}_i$, $\bar{b}_i$, $\bar{\delta}_{1i}$, $\bar{\delta}_{2i}$ are to be chosen later. Defining $\Omega_e(t) = \sum_{i=1}^{2} (\|\tilde{\alpha}_i\|^2 + \|\tilde{\beta}_i\|^2) + |\tilde{X}(t)|^2$, there exist two positive constants θ_{e1}, θ_{e2} holding $\theta_{e1} \Omega_e(t) \le V_e(t) \le \theta_{e2} \Omega_e(t)$. Taking the derivative of $V_e(t)$ along (35)–(39), using Young's inequality and Cauchy–Schwarz inequality, through a lengthy but straightforward calculation, recalling Assumption 2 and choosing

$$\bar{\delta}_{1i} > \frac{2}{\sqrt{q}} \max\left\{ \frac{\sqrt{q}}{2}, \xi_{0i} + \frac{c(1 + \xi_{0i})}{2} \right\},$$

$$\bar{\delta}_{2i} > \frac{2}{\sqrt{q}}\left(-\frac{c}{2\bar{a}_i}+\xi_{0i}+\frac{\bar{b}_i\xi_{0i}}{\bar{a}_i}+\frac{c\xi_{0i}\bar{b}_i}{2\bar{a}_i}\right),$$

$$\bar{a}_i > 4r_0\bar{b}_i+\frac{64|P_2B_i|^2}{q\sqrt{q}\lambda_{\min}(Q_2)},$$

where ξ_{0i} is a sufficiently large positive constant, and large enough positive $\bar{b}_i$ and r_0, we thus obtain

$$\dot{V}_e(t) \le -\sigma_e V_e(t)-\frac{\sqrt{q}}{4}\sum_{i=1}^{2}\bar{a}_i\tilde{\beta}_i(0,t)^2 - \sum_{i=1}^{2}\left(\sqrt{q}-\dot{l}(t)\right)\frac{\bar{b}_i}{2}e^{-\bar{\delta}_{1i}L}\tilde{\alpha}_i(l(t),t)^2, \tag{94}$$

where

$$\sigma_e = \min_{i=1,2}\Bigg\{-\frac{\lambda_{\min}(Q_2)}{2|P_2|},\sqrt{q}\bar{\delta}_{2i}+\frac{c}{\bar{a}_i}-2\xi_{0i}-\frac{2\bar{b}_i\xi_{0i}}{\bar{a}_i\bar{\delta}_{1i}} - \frac{c\xi_{0i}\bar{b}_i}{\bar{a}_i},\sqrt{q}\bar{\delta}_{1i}-\frac{2\xi_{0i}}{\bar{\delta}_{1i}}-c(1+\xi_{0i}) - \frac{2}{r_0}\sqrt{q}F_{1i}e^{\bar{\delta}_{1i}L}-\frac{32L^2|P_2B_i|^2F_{2i}e^{\bar{\delta}_{1i}L}}{\bar{b}_iq\lambda_{\min}(Q_2)}\Bigg\}, \tag{95}$$

with the definition

$$F_{1i}=\max_{y\in[0,L]}\{(\bar{\psi}_i(0,y)+\bar{\phi}_i(0,y))^2\},\ F_{2i}=\max_{y\in[0,L]}\{(\bar{\psi}_i(0,y))^2\}.$$

Note that the decay rate σ_e can be adjusted by the control parameter $\bar{L}$ which affects $\lambda_{\min}(Q_2)$, $\bar{a}_i$ in (95).

Therefore, we obtain the exponential stability result of the target system-$(\tilde{\alpha}_i,\tilde{\beta}_i,\tilde{X})$ in the sense of $\Omega_e(t)$ with the decay rate σ_e. Due to the invertibility of the transformations (33)–(34), the exponential stability with the decay rate at least σ_e of the system-$(\tilde{z}_i,\tilde{w}_i,\tilde{X})$ in the sense of the norm (50) is proved.

Proof of Lemma 3. Differentiating (36) and (37) with respect to x, differentiating (38) and (39) with respect to t, we have

$$\tilde{\alpha}_{ixt}(x,t) = -\sqrt{q}\tilde{\alpha}_{ixx}(x,t)+\frac{c}{2}\tilde{\alpha}_{ix}(x,t) - \frac{c}{2}\tilde{\beta}_{ix}(x,t)+\bar{\eta}_{1i}(x,t), \tag{96}$$

$$\tilde{\beta}_{ixt}(x,t) = \sqrt{q}\tilde{\beta}_{ixx}(x,t)-\frac{c}{2}\tilde{\beta}_{ix}(x,t)+\bar{\eta}_{2i}(x,t), \tag{97}$$

$$\tilde{\alpha}_{ix}(0,t) = \tilde{\beta}_{ix}(0,t)-\frac{c}{\sqrt{q}}\tilde{\beta}_i(0,t)-\frac{1}{\sqrt{q}}\bar{\eta}_{3i}(t) - \left((\bar{\psi}_i(0,0)+\bar{\phi}_i(0,0))-\frac{c}{2\sqrt{q}}\right)\tilde{\alpha}_i(0,t) - \int_0^{l(t)}(\bar{\psi}_{iy}(0,x)+\bar{\phi}_{iy}(0,x))\tilde{\alpha}_i(x,t)dx - \frac{1}{\sqrt{q}}(\dot{l}(t)-\sqrt{q})(\bar{\phi}_i(0,l(t))+\bar{\psi}_i(0,l(t)))\tilde{\alpha}_i(l(t),t), \tag{98}$$

$$\tilde{\beta}_{ix}(l(t),t)=0, \tag{99}$$

where

$$\bar{\eta}_{1i}(x,t)=\int_x^{l(t)}\bar{M}_{ix}(x,y)\tilde{\beta}_i(y,t)dy-\bar{M}_i(x,x)\tilde{\beta}_i(x,t), \tag{100}$$

$$\bar{\eta}_{2i}(x,t)=\int_x^{l(t)}\bar{N}_{ix}(x,y)\tilde{\beta}_i(y,t)dy-\bar{N}_i(x,x)\tilde{\beta}_i(x,t), \tag{101}$$

$$\bar{\eta}_{3i}(t) = -\int_0^{l(t)}(\bar{M}_i(0,x)+\bar{N}_i(0,x))\tilde{\beta}_i(x,t)dx + \int_0^{l(t)}\left(\bar{\psi}_i(0,x)+\bar{\phi}_i(0,x)\right)\left(\int_x^{l(t)}\bar{M}_i(x,y)\tilde{\beta}_i(y,t)dy + \frac{c}{2}\tilde{\alpha}_i(x,t)-\frac{c}{2}\tilde{\beta}_i(x,t)\right)dx. \tag{102}$$

Note: taking the derivative of (39), we have $\dot{l}(t)\tilde{\beta}_x(l(t),t)+\tilde{\beta}_t(l(t),t)=0$. Inserting (37), we obtain $(\dot{l}(t)+\sqrt{q})\tilde{\beta}_x(l(t),t)=0$, which gives to (99).

Applying Cauchy–Schwarz inequality into (100)–(101), there exist two positive constants M_{8i}, M_{9i} such that

$$\|\bar{\eta}_{1i}(\cdot,t)\|^2\le M_{8i}\|\tilde{\beta}_i(\cdot,t)\|^2, \tag{103}$$

$$\|\bar{\eta}_{2i}(\cdot,t)\|^2\le M_{9i}\|\tilde{\beta}_i(\cdot,t)\|^2. \tag{104}$$

According to the exponential stability results proved in Theorem 1, Lemma 5, we know the signals $\bar{\eta}_{3i}(t)$ are exponentially convergent to zero in the sense of

$$|\bar{\eta}_{3i}(t)|\le\lambda_{03}e^{-\bar{\eta}_0t}=\bar{\eta}_{3ma}(t), \tag{105}$$

for $i=1,2$, where the decay rate $\bar{\eta}_0>0$ and $\lambda_{03}>0$ only depends on initial values.

Define a Lyapunov function

$$V_{ieH}(t)=\frac{\breve{a}_i}{2}\int_0^{l(t)}e^{\breve{\delta}_{2i}x}\tilde{\beta}_{ix}(x,t)^2dx+R_4V_e(t) + \frac{\breve{b}_i}{2}\int_0^{l(t)}e^{-\breve{\delta}_{1i}x}\tilde{\alpha}_{ix}(x,t)^2dx+\frac{R_5}{2}\bar{\eta}_{3ma}(t)^2 \tag{106}$$

where the positive constants $\breve{a}_i$, $\breve{b}_i$, $\breve{\delta}_{1i}$, $\breve{\delta}_{2i}$, R_4, R_5 are to be chosen later. Taking the derivative of (106) along (96)–(99), substituting the results of $\dot{V}_e(t)$ (94) in Theorem 1, using Young's inequality and Cauchy–Schwarz inequality and substituting (103)–(104), through a lengthy calculation, we can obtain

$$\dot{V}_{ieH}(t)\le -\frac{R_4\sigma_e}{2}V_e(t)-\left(\frac{1}{2}\sqrt{q}\breve{a}_i-3\sqrt{q}\breve{b}_i\right)\tilde{\beta}_{ix}(0,t)^2 - \left(\left(\frac{1}{2}\sqrt{q}\breve{\delta}_{2i}+\frac{c}{2}-\frac{L}{r_{10i}}\right)\breve{a}_i-\frac{L\breve{b}_ic}{4r_{11i}}\right)\int_0^{l(t)}e^{\breve{\delta}_{2i}x}\tilde{\beta}_{ix}(x,t)^2dx - \left(\frac{1}{2}\sqrt{q}\breve{\delta}_{1i}+\frac{c}{2}-cLr_{11i}-\frac{L}{r_{12i}}\right)\breve{b}_i\int_0^{l(t)}e^{-\breve{\delta}_{1i}x}\tilde{\alpha}_{ix}(x,t)^2dx - \frac{(\sqrt{q}-\dot{l}(t))\breve{b}_ie^{-\breve{\delta}_{1i}L}}{2}\tilde{\alpha}_{ix}(l(t),t)^2 - \left(\frac{R_4}{2}\sigma_e\theta_{e1}-6\breve{b}_i\sqrt{q}\left(2M_{7i}+\frac{c^2}{2q}\right)LM_{7i}-3\breve{b}_i\sqrt{q}\hat{M}_{7i}L\right)\|\tilde{\alpha}_i(\cdot,t)\|^2 - \left(\frac{R_4}{2}\sigma_e\theta_{e1}-\frac{M_{8i}r_{12i}\breve{b}_iL}{4}-\frac{M_{9i}\breve{a}_ir_{10i}e^{\breve{\delta}_{2i}L}L}{4}\right)\|\tilde{\beta}_i(\cdot,t)\|^2 - \left(R_5\bar{\eta}_0-\frac{3\breve{b}_i}{\sqrt{q}}\right)\bar{\eta}_{3ma}(t)^2 - \left(\frac{R_4}{4}\sqrt{q}\bar{a}_i-\frac{3\breve{b}_ic^2}{\sqrt{q}}-6\breve{b}_i\sqrt{q}\left(2M_{7i}+\frac{c^2}{2q}\right)\right)\tilde{\beta}_i(0,t)^2 - \left(R_4(\sqrt{q}-\dot{l}(t))\frac{\bar{b}_ie^{-\bar{\delta}_{1i}L}}{2}-\frac{3\breve{b}_i(\dot{l}(t)-\sqrt{q})^2M_{7i}}{\sqrt{q}}\right)\tilde{\alpha}_i(l(t),t)^2, \tag{107}$$

where (38) and (105) are used. r_{10i}, r_{11i}, r_{12i} are positive constants from using Young's inequality, and $M_{7i}=\max_{0\le x\le L}\{(\bar{\psi}_i(0,x)+\bar{\phi}_i(0,x))^2\}$, $\hat{M}_{7i}=\max_{0\le x\le L}\{(\bar{\psi}_{iy}(0,x)+\bar{\phi}_{iy}(0,x))^2\}$.

Recalling Assumption 2 and choosing $\breve{\delta}_{1i}$, $\breve{\delta}_{2i}$, $\breve{a}_i$ to satisfy

$$\breve{\delta}_{1i}>\frac{2}{\sqrt{q}}\left(cLr_{11i}+\frac{L}{r_{12i}}-\frac{c}{2}\right),\ \breve{\delta}_{2i}>\frac{2}{\sqrt{q}}\left(\frac{L}{r_{10i}}-\frac{c}{2}\right),$$

$$\breve{a}_i>6\breve{b}_i,$$

with large enough r_{11i}, R_4, R_5 and arbitrary $\check{b}_i, r_{10i}, r_{12i}$, we thus arrive at $\dot{V}_{ieH}(t) \leq -\sigma_{ieH} V_{ieH}(t)$ where $\sigma_{ieH} > 0$.

Defining a Lyapunov function $V_{eH}(t) = V_{1eH}(t) + V_{2eH}(t)$, taking the derivative of $V_{eH}(t)$, we have

$$\dot{V}_{eH}(t) \leq -\sigma_{eH} V_{eH}(t), \tag{108}$$

where

$$\sigma_{eH} = \min_{i=1,2}\Bigg\{\sqrt{q}\check{\delta}_{2i} + c - \frac{2L}{r_{10i}} - \frac{L\check{b}_i c}{2\check{a}_i r_{11i}}, \sqrt{q}\check{\delta}_{1i} + c - 2cLr_{11i} - \frac{2L}{r_{12i}}, 2\bar{\eta}_0 - \frac{6\check{b}_i}{\sqrt{q}R_5}, \frac{\sigma_e}{2}\Bigg\}. \tag{109}$$

Note that the decay rate σ_{eH} can be adjusted by the control parameter $\bar{L}$ which affects σ_e.

We thus obtain the exponential stability estimate in the sense of $\|\tilde{\alpha}_{1x}(\cdot,t)\|^2 + \|\tilde{\beta}_{1x}(\cdot,t)\|^2 + \|\tilde{\alpha}_{2x}(\cdot,t)\|^2 + \|\tilde{\beta}_{2x}(\cdot,t)\|^2$. Due to the invertibility of the transformation (33)–(34), we can obtain the exponential stability estimate in the sense of (52) with the decay rate al least $\sigma_{eHf} = \min\{\sigma_e, \sigma_{eH}\}$. The proof of Lemma 3 is completed.

Proof of Lemma 4. The kernel equations have the same form as the kernel equations (17)–(23) in Di Meglio et al. (2018). In detail, (65)–(66) are two coupled linear hyperbolic PDEs which correspond to (17)–(18) in Di Meglio et al. (2018) by setting $m = n = 1$ and replacing the K, L as ψ_i, ϕ_i. Boundary conditions (68),(67) correspond to (19),(21) in Di Meglio et al. (2018). The ODE (69) with the initial condition (70) correspond to (22) with (23) in Di Meglio et al. (2018). Because the well-posedness of (17)–(23) in Di Meglio et al. (2018) has been proved, under the boundedness and enough regularity assumptions (Assumptions 1 and 2) on the time-varying domain $l(t)$, Lemma 4 can then be proved.

Proof of Lemma 5. We establish the stability proof of the target system-$(\alpha_1, \beta_1, \alpha_2, \beta_2, \hat{X})$ via Lyapunov analysis. The equivalent stability property between the target system and the observer system-$(\hat{z}_1, \hat{w}_1, \hat{z}_2, \hat{w}_2, \hat{X})$ is ensured due to the invertibility of the backstepping transformation (53)–(54).

Step.1 Consider now a Lyapunov function for the system-$(\alpha_1, \beta_1, \alpha_2, \beta_2, \hat{X})$:

$$V_i(t) = \hat{X}^T(t) P_1 \hat{X}(t) + \frac{a_i}{2}\int_0^{l(t)} e^{\delta_{i2}x}\beta_i(x,t)^2 dx + \frac{b_i}{2}\int_0^{l(t)} e^{-\delta_{i1}x}\alpha_i(x,t)^2 dx, \tag{110}$$

where the matrix $P_1 = P_1^T > 0$ is the solution to the Lyapunov equation $P_1\acute{A} + \acute{A}^T P_1 = -Q_1$, for some $Q_1 = {Q_1}^T > 0$. The positive parameters $a_i, b_i, \delta_{i1}, \delta_{i2}$ are to be chosen later. Defining $\Omega_{1i}(t) = \|\beta_i(\cdot,t)\|^2 + \|\alpha_i(\cdot,t)\|^2 + |\hat{X}(t)|^2$, we have $\theta_{11i}\Omega_{1i}(t) \leq V_i(t) \leq \theta_{12i}\Omega_{1i}(t)$, where $\theta_{11i} = \min\left\{\lambda_{\min}(P_1), \frac{a_i}{2}, \frac{b_i e^{-\delta_{i1}L}}{2}\right\} > 0$ and $\theta_{12i} = \max\left\{\lambda_{\max}(P_1), \frac{a_i e^{\delta_{i2}L}}{2}, \frac{b_i}{2}\right\} > 0$.

Taking the derivative of $V_i(t)$ along the (55)–(59), applying Young's inequality, and choosing the parameters $b_i, \delta_{i1}, \delta_{i2}$ to satisfy

$$0 < b_i < \frac{\lambda_{\min}(Q_1)}{2\sqrt{q}\left|\bar{D}_i\right|^2},\ \delta_{i2} > \frac{4\xi_i b_i}{a_i\sqrt{q}} + \frac{a_i\lambda_i}{r_{2i}\sqrt{q}},\ \delta_{i1} > \frac{1}{\sqrt{q}}\max\left\{\sqrt{q}, 6\xi_i + \frac{2\xi_i^2 b_i}{\lambda_{\min}(Q_1)} + 2c\right\},$$

with small enough positive constants r_{4i}, r_{3i}, we thus obtain

$$\begin{aligned}\dot{V}_i(t) \leq & -\sigma_i V_i(t)\\ & - \left(\frac{\sqrt{q}}{2}a_i - \frac{3\sqrt{q}}{2}b_i - \frac{4\left|P_1 B_i\right|}{q\lambda_{\min}(Q_1)}\right)\beta_i(0,t)^2\\ & - \left(\frac{\sqrt{q}}{2}b_i e^{-\delta_{i1}l(t)} - \dot{l}(t)\frac{b_i}{2}e^{-\delta_{i1}l(t)}\right)\alpha_i(l(t),t)^2\\ & + \left(\frac{r_{2i}e^{\delta_{i2}L}\bar{\lambda}_i}{2} + \frac{4\left|P_1 B_j\right|}{q\lambda_{\min}(Q_1)}\right)\beta_j(0,t)^2\\ & + \left(\frac{a_i^2 e^{\delta_{i2}L}L}{r_{4i}}H_i + \frac{b_i^2 L}{2r_{3i}}G_i\right)\tilde{z}_i(l(t),t)^2\\ & + \left(\frac{3\sqrt{q}b_i}{2}|D_i|^2 + \frac{a_i^2 e^{\delta_{i2}L}L}{r_{4i}}Y_i\right)\left|\tilde{X}(t)\right|^2,\end{aligned} \tag{111}$$

where ξ_i are sufficiently large constants, and

$$\begin{aligned}\sigma_i = & \frac{1}{\theta_{12i}}\min\Bigg\{\frac{3}{4}\lambda_{\min}(Q_1) - \frac{3\sqrt{q}b_i}{2}\left|\bar{D}_i\right|^2, \left(\frac{\sqrt{q}}{2}\delta_{i2} + \frac{c}{2}\right)a_i\\ & - \xi_i b_i\left(1 + \frac{1}{\delta_{i1}}\right) - \frac{a_i^2\bar{\lambda}_i}{2r_{2i}} - \frac{r_{4i}(H_i + Y_i)}{2}, \left(\left(\frac{\sqrt{q}}{2}\delta_{i1} - c\right)b_i\right.\\ & \left. - \frac{2\xi_i b_i}{\delta_{i1}} - \xi_i b_i - \frac{\xi_i^2 b_i^2}{\lambda_{\min}(Q_1)} - \frac{r_{3i}G_i}{2}\right)e^{-\delta_{i1}L}\Bigg\}.\end{aligned} \tag{112}$$

a_i, r_{2i} would be chosen later. $H_i, Y_i, G_i, \bar{\lambda}_i$ are defined as

$$H_i = \max\left\{\left|\mathcal{N}_i(x,t)\right|\right\}, Y_i = \max\left\{\left|\mathcal{N}_{1i}(x)\right|\right\}, \tag{113}$$

$$G_i = \max\left\{\left|\bar{\Gamma}_i(x,t)\right|\right\}, \bar{\lambda}_i = \max\{|\lambda_i(x)|\}, \tag{114}$$

for $x \in [0, L]$, $t \in [0, \infty)$.

Step.2 Recalling the exponential stability result in the sense of $\|\tilde{z}_i(\cdot,t)\|, \|\tilde{w}_i(\cdot,t)\|, |\tilde{X}(t)|$ and $\|\tilde{z}_{ix}(\cdot,t)\|, \|\tilde{w}_{ix}(\cdot,t)\|$ proved in Lemmas 2 and 3, considering $\tilde{w}_i(l(t),t) = 0$ in (32), using Cauchy–Schwarz inequality, similarly to (81), we can arrive at that $\tilde{w}_i(0,t)$ is exponentially convergent to zero. Recalling $\tilde{w}_i(0,t) + \tilde{z}_i(0,t) = 0$ in (32) and using Cauchy–Schwarz inequality again, similarly to (82), we have $\tilde{z}_i(l(t),t)$ is exponentially convergent. Then we have that signals $\tilde{X}(t)$ and $\tilde{z}_i(l(t),t)$ are exponentially convergent to zero in the sense of

$$\max\left\{\left|\tilde{z}_i(l(t),t)\right|, \left|\tilde{X}(t)\right|\right\} \leq \lambda_0 e^{-\eta t} = \check{\eta}_m(t), \tag{115}$$

for $i = 1, 2$, where the decay rate $\eta > 0$ and λ_0 is a positive constant which depends on initial conditions only.

Now, we consider a Lyapunov function candidate for the whole target system-$(\alpha_1, \beta_1, \alpha_2, \beta_2, \hat{X})$

$$V(t) = \sum_{i=1}^{2} V_i(t) + R\check{\eta}_m(t)^2, \tag{116}$$

where $R > 0$ to be determined later. Defining $\Omega_a(t) = \|\beta_1(\cdot,t)\|^2 + \|\alpha_1(\cdot,t)\|^2 + \|\beta_2(\cdot,t)\|^2 + \|\alpha_2(\cdot,t)\|^2 + |\hat{X}(t)|^2 + \check{\eta}_m(t)^2$, we have $\theta_{a1}\Omega_a(t) \leq V(t) \leq \theta_{a2}\Omega_a(t)$ with two positive constants θ_{a1}, θ_{a2}.

Taking the derivative of (116) and considering (111), we get

$$\begin{aligned}\dot{V}(t) \leq & -\sum_{i=1}^{2}\Bigg[\left(\sqrt{q} - \dot{l}(t)\right)\frac{b_i}{2}e^{-\delta_{i1}l(t)}\alpha_i(l(t),t)^2\\ & + \left(\frac{\sqrt{q}}{2}a_i - \frac{3\sqrt{q}}{2}b_i - \frac{8\left|P_1 B_i\right|}{q\lambda_{\min}(Q_1)} - \frac{r_{2j}e^{\delta_{j2}L}\bar{\lambda}_j}{2}\right)\beta_i(0,t)^2\\ & + \left(\frac{R}{2}\eta - \frac{a_i^2 e^{\delta_{i2}L}}{r_{4i}}H_i - \frac{b_i^2 L}{2r_{3i}}G_i\right)\check{\eta}_m(t)^2 + \sigma_i V_i(t)\\ & + \left(\frac{R}{2}\eta - \frac{3\sqrt{q}b_i}{2}|D_i|^2 - \frac{a_i^2 e^{\delta_{i2}L}L}{r_{4i}}Y_i\right)\check{\eta}_m(t)^2\Bigg].\end{aligned} \tag{117}$$

Note that (115) is used to replace $\tilde{z}_i(l(t),t)^2$ and $|\tilde{X}(t)|^2$ in the last two lines of (111) as $\check{\eta}_m(t)^2$ respectively. We can choose

$$a_i > 3b_i + \frac{16\,|P_1B_i|}{q\sqrt{q}\lambda_{\min}(Q_1)} + \frac{r_{2j}e^{\delta_{j2}L}\bar{\lambda}_j}{2}, \tag{118}$$

with some positive r_{2j} which is adjustable, and choose large enough R to make sure the coefficients before $\check{\eta}_m(t)^2$ positive. Recalling Assumption 2, i.e., $\dot{l}(t) < \sqrt{q}$, the coefficients of the $\alpha_i(l(t),t)^2$ in (117) are positive in all ascending ($\dot{l}(t) < 0$), descending ($\dot{l}(t) > 0$) and stop ($\dot{l}(t) = 0$) cases. We thus arrive at

$$\dot{V}(t) \le -\sigma V(t) - \sum_{i=1}^{2} \bar{s}_i \beta_i(0,t)^2, \tag{119}$$

where $\bar{s}_i > 0$ and

$$\sigma = \min\Bigg\{\sigma_1, \sigma_2, \frac{1}{R}\sum_{i=1}^{2}\Bigg(R\eta - \frac{3\sqrt{q}b_i}{2}|D_i|^2 - \frac{a_i^2e^{\delta_{i2}L}L}{r_{4i}}Y_i - \frac{a_i^2e^{\delta_{i2}L}L}{r_{4i}}H_i - \frac{b_i^2L}{2r_{3i}}G_i\Bigg)\Bigg\} > 0. \tag{120}$$

Recalling σ_i (112), we know the decay rate σ can be adjusted by the control parameters κ_i which affect σ_i and H_i, Y_i, G_i in (120) through $\lambda_{\min}(Q_1)$, $\bar{D}_i$, γ_i, ϕ_i, ψ_i, and the control parameter $\bar{L}$ which would affect η in (120).

Therefore, we obtain the exponential stability result in the sense of $\|\alpha_i(\cdot,t)\|^2 + \|\beta_i(\cdot,t)\|^2 + |\hat{X}(t)|^2$. Due to the invertibility of the transformations (53)–(54), the exponential stability with the decay rate at least σ of the system-$(\hat{z}_i, \hat{w}_i, \hat{X})$ in the sense of the norm (75) in Lemma 5 is proved.

Proof of Lemma 6. Differentiating (56) and (57) with respect to x, differentiating (58) and (59) with respect to t, we have

$$\alpha_{ixt}(x,t) = -\sqrt{q}\alpha_{ixx}(x,t) - c\beta_{ix}(x,t) - c\alpha_{ix}(x,t) + \eta_{i1}(x,t), \tag{121}$$

$$\beta_{ixt}(x,t) = \sqrt{q}\beta_{ixx}(x,t) - \lambda_i'(x)\beta_j(0,t) - \frac{c}{2}\beta_{ix}(x,t) + \eta_{i2}(x,t), \tag{122}$$

$$\alpha_{ix}(0,t) = \beta_{ix}(0,t) + \sum_{f=1}^{2}\frac{B_f}{q}\left(\bar{D}_i\beta_f(0,t) + D_i\tilde{\beta}_f(0,t)\right)$$

$$\frac{c}{2\sqrt{q}}\beta_i(0,t) + \frac{1}{\sqrt{q}}\lambda_i(0)\beta_j(0,t) + \frac{1}{\sqrt{q}}\eta_{i3}(t), \tag{123}$$

$$\beta_{ix}(l(t),t) = \frac{\lambda_i(l(t))}{\dot{l}(t)+\sqrt{q}}\beta_j(0,t) + \frac{c}{2(\dot{l}(t)+\sqrt{q})}\beta_i(0,t) + \frac{\mathcal{N}_i(l(t),t)}{\dot{l}(t)+\sqrt{q}}\tilde{z}_i(l(t),t) + \frac{\mathcal{N}_{1i}(l(t))}{\dot{l}(t)+\sqrt{q}}\tilde{X}(t), \tag{124}$$

where

$$\eta_{i1}(x,t) = c\int_0^x \psi_{ix}{}^I(x,y)\alpha_i(y,t)dy + c\gamma_i'{}^I(x)\hat{X}(t) + c\int_0^x \phi_{ix}{}^I(x,y)\beta_i(y,t)dy + c\psi_i{}^I(x,x)\alpha_i(x,t) + c\phi_i{}^I(x,x)\beta_i(x,t) + \bar{\Gamma}_i'(x,t)\tilde{z}_i(l(t),t), \tag{125}$$

$$\eta_{i2}(x,t) = -\mathcal{N}_{1i}'(x)\tilde{X}(t) - \mathcal{N}_i'(x,t)\tilde{z}_i(l(t),t), \tag{126}$$

$$\eta_{i3}(t) = \left[\bar{D}_i\left(\bar{A} + \sum_{i=f}^{2}B_f\kappa_f\right) - c\gamma_i{}^I(0) + c\bar{D}_i\right]\hat{X}(t) + \left(\bar{D}_i\bar{L}(C_1+C_2) + cD_i + D_i\hat{A} + \mathcal{N}_{1i}(0)\right)\tilde{X}(t) - \frac{1}{\sqrt{q}}(\bar{\Gamma}_i(0,t) - \Gamma_i(0,t))\tilde{z}_i(l(t),t) + D_i\sum_{f=1}^{2}\frac{B_f}{\sqrt{q}}\int_0^{l(t)}\bar{\psi}_f(y)\tilde{\alpha}_f(y,t)dy. \tag{127}$$

Applying Cauchy–Schwarz inequality into (125)–(126), there exist positive constants $N_{1i}, N_{2i}, N_{3i}, N_{4i}, N_{5i}, N_{6i}$ such that

$$\|\eta_{i1}(\cdot,t)\|^2 \le N_{1i}\|\alpha_i(\cdot,t)\|^2 + N_{2i}\left|\hat{X}(t)\right|^2 + N_{3i}\|\beta_i(\cdot,t)\|^2 + N_{4i}\tilde{z}_i(l(t),t)^2, \tag{128}$$

$$\|\eta_{i2}(\cdot,t)\|^2 \le N_{5i}\tilde{z}_i(l(t),t)^2 + N_{6i}\left|\tilde{X}(t)\right|^2. \tag{129}$$

According to (115), we know $\tilde{z}_i(l(t),t)$ is exponentially convergent to zero with the decay rate η. According to the exponential stability results proved in Lemma 2, Lemma 5, we have the signals $\eta_{i3}(t)$ are exponentially convergent to zero in the sense of

$$|\eta_{i3}(t)| \le \lambda_{03i}e^{-\eta_{0i}t} = \eta_{ima}(t) \tag{130}$$

where $\lambda_{03i} > 0$ only depend on initial values and the decay rate $\eta_{0i} > 0$.

Define a Lyapunov function

$$V_H(t) = \sum_{i=1}^{2}\left[\frac{\hat{a}_i}{2}\int_0^{l(t)}e^{\hat{\delta}_{2i}x}\beta_{ix}(x,t)^2dx + \frac{\hat{b}_i}{2}\int_0^{l(t)}e^{-\hat{\delta}_{1i}x}\alpha_{ix}(x,t)^2dx + \frac{R_3}{2}\eta_{ima}(t)^2\right] + R_2\check{\eta}_m(t)^2 + R_1V(t) + R_0V_e(t), \tag{131}$$

where positive constants $\hat{a}_i$, $\hat{b}_i$, $\hat{\delta}_{1i}$, $\hat{\delta}_{2i}$, R_0, R_1, R_2, R_3 would be determined later. Taking the derivative of (131) along (121)–(124), using Young's and Cauchy–Schwarz inequalities, substituting the results of $\dot{V}(t)$ (119), $\dot{V}_e(t)$ (94) and substituting (128)–(129), recalling Assumption 2, through a lengthy calculation, we can obtain

$$\begin{aligned}\dot{V}_H(t) \le{}& -\frac{R_1}{2}\sigma V(t) + \sum_{i=1}^{2}\Bigg[-\left(\frac{\sqrt{q}\hat{a}_i}{2} - 4\sqrt{q}\hat{b}_i\right)\beta_{ix}(0,t)^2 \\ &- \left(\left(\frac{1}{2}\sqrt{q}\hat{\delta}_{2i} + \frac{c}{2} - \frac{1}{r_{6i}} - \frac{1}{r_{10i}}\right)\hat{a}_i - \frac{r_{7i}\hat{b}_ic}{4}\right)\int_0^{l(t)}e^{\hat{\delta}_{2i}x}\beta_{ix}(x,t)^2dx - \left(\frac{1}{2}\sqrt{q}\hat{\delta}_{1i} + c - \frac{c}{r_{7i}} - \frac{1}{r_{8i}}\right)\hat{b}_i\int_0^{l(t)}e^{-\hat{\delta}_{1i}x}\alpha_{ix}(x,t)^2dx \\ &- \left(\frac{R_1\sigma\theta_{a1}}{4} - \frac{r_{8i}\hat{b}_iN_{1i}}{4}\right)\|\alpha_i(\cdot,t)\|^2 - \left(\frac{R_1\sigma\theta_{a1}}{4} - \frac{r_{8i}\hat{b}_iN_{3i}}{4}\right)\|\beta_i(\cdot,t)\|^2 - \left(\frac{R_1\sigma\theta_{a1}}{4} - \frac{r_{8i}\hat{b}_iN_{2i}}{4}\right)\left|\hat{X}(t)\right|^2 - \left(R_3\eta_{0i} - \frac{4\hat{b}_i}{\sqrt{q}}\right)\eta_{ima}(t)^2 \\ &- \left(R_2\eta - \frac{a_ir_{6i}e^{\hat{\delta}_{2i}L}N_{5i}}{4} - \frac{r_{8i}\hat{b}_iN_{4i}}{4} - \frac{2(\sqrt{q}+\bar{v}_{\max})\hat{a}_ie^{e^{\hat{\delta}_{2i}L}}H_i^2}{(\sqrt{q}-\bar{v}_{\max})^2}\right)\check{\eta}_m(t)^2 - \left(\frac{R_1}{4}\bar{s}_i - \frac{16\hat{r}_bB_i^2}{q\sqrt{q}} - \frac{16}{\sqrt{q}}\hat{\lambda} - \frac{\lambda_mL}{4} - \frac{2(\sqrt{q}+\bar{v}_{\max})\hat{a}_\lambda}{(\sqrt{q}-\bar{v}_{\max})^2} - \frac{(\sqrt{q}+\bar{v}_{\max})\hat{a}_ie^{\hat{\delta}_{2i}L}c^2}{2(\sqrt{q}-\bar{v}_{\max})^2}\right)\beta_i(0,t)^2 - \left(\frac{R_1\sigma\theta_{a1}}{4}\right.\end{aligned}$$

$$- \frac{a_i r_{6i} e^{\hat{\delta}_{2i} L} N_{6i}}{4} - \frac{2(\sqrt{q} + \bar{v}_{\max}) \hat{a}_i e^{\hat{\delta}_{2i} L} Y_i^2}{(\sqrt{q} - \bar{v}_{\max})^2} \Big) \Big| \tilde{X}(t) \Big|^2$$
$$- \left(R_0 \frac{\sqrt{q}}{4} \bar{a}_i - \frac{16 \hat{r_a} B_i^2}{q\sqrt{q}} \right) \tilde{\beta}_i(0,t)^2 \Big] - R_0 \sigma_e V_e(t) \tag{132}$$

where for $i = 1, 2$, $\hat{\lambda} = \max\{\frac{c^2}{4}\hat{b}_i, \lambda_i(0)^2 \hat{b}_i\}$, $\lambda_m = \max_{0\le x\le L}\{a_i r_{10i} e^{\delta_{2i} L} \lambda_i'(x)^2\}$, $\hat{r_b} = \max\{\hat{b}_i \bar{D}_i^2\}$, $\hat{r_a} = \max\{\hat{b}_i D_i^2\}$, and $\hat{a}_\lambda = \max_{0\le l(t)\le L}\{\hat{a}_i e^{\hat{\delta}_{2i} L} \lambda_i(l(t))^2\}$. Note that (115) and (130) are used to replace $\tilde{z}_i(l(t),t)^2$ and $\eta_{i3}(t)^2$ with positive signs as $\check{\eta}_m(t)^2$ and $\eta_{ima}(t)^2$ respectively. H_i, Y_i are shown in (113). From using Young's inequality, r_{6i}, r_{7i}, r_{8i}, r_{10i} are arbitrary positive constants. Choose positive constants $\hat{a}_i$, $\hat{\delta}_{1i}$, $\hat{\delta}_{2i}$ satisfying

$$\hat{a}_i > 8\hat{b}_i, \quad \hat{\delta}_{1i} > \frac{2}{\sqrt{q}} \left(-c + \frac{c}{r_{7i}} + \frac{1}{r_{8i}} \right), \tag{133}$$

$$\hat{\delta}_{2i} > \frac{r_{7i} \hat{b}_i c}{2\hat{a}_i \sqrt{q}} - \frac{c}{\sqrt{q}} + \frac{2}{\sqrt{q} r_{6i}} + \frac{2}{\sqrt{q} r_{10i}}, \tag{134}$$

with large enough R_0, R_1, R_2, R_3 and arbitrary $\hat{b}_i$, and then we arrive at

$$\dot{V}_H(t) \le -\sigma_H V_H(t), \tag{135}$$

where

$$\sigma_H = \min_{i=1,2} \Bigg\{ \frac{1}{2}\sigma, \sigma_e, \sqrt{q}\hat{\delta}_{2i} + c - \frac{2}{r_{6i}} - \frac{2}{r_{10i}} - \frac{r_{7i}\hat{b}_i c}{2\hat{a}_i},$$
$$\sqrt{q}\hat{\delta}_{1i} + 2c - \frac{2c}{r_{7i}} - \frac{2}{r_{8i}}, R_3\eta_{0i} - \frac{4\hat{b}_i}{R_3\sqrt{q}}, \eta - \frac{a_i r_{6i} e^{\hat{\delta}_{2i} L} N_{5i}}{2R_2}$$
$$- \frac{r_{8i}\hat{b}_i N_{4i}}{2R_2} - \frac{4(\sqrt{q} + \bar{v}_{\max})\hat{a}_i e^{\hat{\delta}_{2i} L} H_i^2}{(\sqrt{q} - \bar{v}_{\max})^2 R_2} \Bigg\} > 0. \tag{136}$$

Note that σ_H can be adjusted by the control parameters κ_i which affect σ and L which affects η, η_{0i}, σ_e.

We thus obtain the exponential stability estimate in the sense of $\|\alpha_{ix}(\cdot,t)\|^2 + \|\beta_{ix}(\cdot,t)\|^2$. Differentiating (62)–(63) with respect to x, using Young's and Cauchy–Schwarz inequalities, we have

$$\|\hat{z}_{ix}\|^2 \equiv \|\alpha_{ix}(\cdot,t)\|^2,$$
$$\|\hat{w}_{ix}\|^2 \le 6\big(\|\beta_{ix}(\cdot,t)\|^2 + \bar{K}_\infty \|\alpha_i(\cdot,t)\|^2$$
$$+ \bar{L}_\infty \|\beta_i(\cdot,t)\|^2 + \|\gamma_i^I(\cdot)'\|^2 \Big|\hat{X}(t)\Big|^2\big).$$

where $\bar{K}_\infty = \max_{x\in[0,L], y\in[0,L]}\{L^2\psi_{ix}^I(x,y)^2 + \psi_i^I(x,x)^2\}$ and $\bar{L}_\infty = \max_{x\in[0,L], y\in[0,L]}\{L^2\phi_{ix}^I(x,y)^2 + \phi_i^I(x,x)^2\}$.

Considering the exponential stability result in sense of $\|\alpha_i(\cdot,t)\|^2 + \|\beta_i(\cdot,t)\|^2 + |\hat{X}(t)|^2$ proved in Lemma 5 and $\|\alpha_{ix}(\cdot,t)\|^2 + \|\beta_{ix}(\cdot,t)\|^2$ proved above, we can obtain the exponential stability estimate of the system-$(\hat{z}_i, \hat{w}_i)$ in the sense of (76) with the decay rate at least $\sigma_f = \min\{\sigma, \sigma_H\}$.

References

Aamo, O. (2013). Disturbance Rejection in 2 ×2 Linear Hyperbolic Systems. *IEEE Transactions on Automatic Control*, *58*(5), 1095–1106.

Anfinsen, H., & Aamo, O. M. (2015). Disturbance rejection in the interior domain of linealr 2 ×2 hyperbolic systems. *IEEE Transactions on Automatic Control*, *60*(1), 186–191.

Anfinsen, H., & Aamo, O. M. (2017a). Adaptive output-feedback stabilization of linear 2 ×2 hyperbolic systems using anti-collocated sensing and control. *Systems & Control Letters*, *104*, 86–94.

Anfinsen, H., & Aamo, O. M. (2017b). Disturbance rejection in general heterodirectional 1-D linear hyperbolic systems using collocated sensing and control. *Automatica*, *76*, 230–242.

Anfinsen, H., & Aamo, O. M. (2018). Adaptive control of linear 2 ×2 hyperbolic systems. *Automatica*, *87*, 69–82.

Anfinsen, H., Diagne, M., Aamo, O. M., & Krstic, M. (2017). Estimation of boundary parameters in general heterodirectional linear hyperbolic systems. *Automatica*, *79*, 185–197.

Basturk, H. I., & Krstic, M. (2014). State derivative feedback for adaptive cancellation of unmatched disturbances in unknown strict-feedback LTI systems. *Automatica*, *50*, 2539–2545.

Bin, M., & Di Meglio, F. (2017). Boundary estimation of boundary parameters for linear hyperbolic PDEs. *IEEE Transactions on Automatic Control*, *62*(8), 3890–3904.

Coron, J. M., Vazquez, R., Krstic, M., & Bastin, G. (2013). Local exponential H^2 stabilization of a 2 ×2 quasilinear hyperbolic system using backstepping. *SIAM Journal on Control and Optimization*, *51*(3), 2005–2035.

Deutscher, J. (2017a). Backstepping Design of Robust State Feedback Regulators for Linear 2 ×2 Hyperbolic Systems. *IEEE Transactions on Automatic Control*, *62*(10), 5240–5257.

Deutscher, J. (2017b). Finite-time output regulation for linear 2 ×2 hyperbolic systems using backstepping. *Automatica*, *75*, 54–62.

Deutscher, J. (2017c). Output regulation for general linear heterodirectional hyperbolic systems with spatially-varying coefficients. *Automatica*, *85*, 34–42.

Deutscher, J., Gehring, N., & Kern, R. (2018). Output feedback control of general linear heterodirectional hyperbolic PDE-ODE systems with spatially-varying coefficients. *International Journal of Control*, 1–17. http://dx.doi.org/10.1080/00207179.2018.1436770.

Di Meglio, F., Bribiesca, F., Hu, L., & Krstic, M. (2018). Stabilization of coupled linear heterodirectional hyperbolic PDE-ODE systems. *Automatica*, *87*, 281–289.

Di Meglio, F., Vazquez, R., & Krstic, M. (2013). Stabilization of a system of $n + 1$ coupled first-order hyperbolic linear PDEs with a single boundary input. *IEEE Transactions on Automatic Control*, *58*(12), 3097–3111.

Gugat, M. (2007a). Optimal boundary feedback stabilization of a string with moving boundary. *IMA Journal of Mathematical Control and Information*, *25*, 111–121.

Gugat, M. (2007b). Optimal energy control in finite time by varying the length of the string. *SIAM Journal on Control and Optimization*, *46*, 1705–1725.

Gugat, M. (2014). Boundary feedback stabilization of the telegraph equation: Decay rates for vanishing damping term. *Systems & Control Letters*, *66*, 72–84.

Hasan, A., Aamo, O., & Krstic, M. (2016). Boundary observer design for hyperbolic PDE-ODE cascade systems. *Automatica*, *68*, 75–86.

Hu, L., Di Meglio, F., Vazquez, R., & Krstic, M. (2016). Control of homodirectional and general heterodirectional linear coupled hyperbolic PDEs. *IEEE Transactions on Automatic Control*, *61*(11), 3301–3314.

Krstic, M. (2009). *Delay compensation for nonlinear, adaptive, and PDE systems*. Springer.

Krstic, M., & Smyshlyaev, A. (2008). *Boundary control of PDEs: A course on backstepping designs*. Singapore: Siam.

Logemann, H., Rebarber, R., & Weiss, G. (1996). Conditions for robustness and nonrobustness of the stability of feedback systems with respect to small delays in the feedback loop. *SIAM Journal on Control and Optimization*, *34*(2), 572–600.

Roman, C., Bresch-Pietri, D., Cerpa, E., Prieur, C., & Sename, O. (2016). Backstepping observer based-control for an anti-damped boundary wave PDE in presence of in-domain viscous damping. In *55th conference on decision and control (CDC)*.

Roman, C., Bresch-Pietri, D., Prieur, C., & Sename, O. (2016). Robustness of an adaptive output feedback for an anti-damped boundary wave PDE in presence of in-domain viscous damping. In *American control conference (ACC)*.

Su, L., Wang, J.-M., & Krstic, M. (2018). Boundary Feedback Stabilization of a Class of Coupled Hyperbolic Equations with Non-local Terms. *IEEE Transactions on Automatic Control*, *63*, 2633–2640.

Vazquez, R., Krstic, M., & Coron, J. M. (2011). Backstepping boundary stabilization and state estimation of a 2 ×2 linear hyperbolic system. In *Decision and control and European control conference (CDC-ECC), 50th IEEE conference on* (pp. 4937–4942).

Wang, J., Koga, S., Pi, Y., & Krstic, M. (2018). Axial vibration suppression in a PDE Model of ascending mining cable elevator. *Journal of Dynamic Systems, Measurement, and Control*, *140*, 111003.

Wang, J., Krstic, M., & Pi, Y. (2018). Control of a 2×2 coupled linear hyperbolic system sandwiched between 2 ODEs. *International Journal of Robust and Nonlinear Control*, *28*(2), 3987–4016.

Wang, J., Pi, Y., Hu, Y., & Gong, X. (2017). Modeling and dynamic behavior analysis of a coupled multi-cable double drum winding hoister with flexible guides. *Mechanism and Machine Theory*, *108*, 191–208.

Wang, J., Tang, S.-X., Pi, Y., & Krstic, M. (2017). Disturbance estimation of a wave PDE on a time-varying domain. In *2017 proceedings of the conference on control and its applications* (pp. 107–111). Society for Industrial and Applied Mathematics.

Wang, J., Tang, S.-X., Pi, Y., & Krstic, M. (2018). Exponential regulation of the anti-collocatedly disturbed cage in a wave PDE-modeled ascending cable elevator. *Automatica*, *95*, 122–136.

Yu, H., Vazquez, R., & Krstic, M. (2017). Adaptive output feedback for hyperbolic PDE pairs with non-local coupling. In *American control conference IEEE* (pp. 487–492).

Ji Wang received the Ph.D. degree in Mechanical Engineering from Chongqing University, Chongqing, China, in 2018. He was a visiting graduate student in the Department of Mechanical and Aerospace Engineering at University of California, San Diego, La Jolla, CA, USA, from 2015 to 2017. His research interests include modeling and control of distributed parameter systems, active disturbance rejection control and adaptive control, with applications in mechanical systems.

Yangjun Pi received the B.Eng. degree in Mechatronic Engineering and the Ph.D. degree in Mechanical Engineering from Zhejiang University, Hangzhou, China, in 2005 and 2010 respectively. Currently, he is an Associate Professor in the State Key Laboratory of Mechanical Transmission, Chongqing University, Chongqing, China. His research interests include control of distributed parameter systems, vibration control.

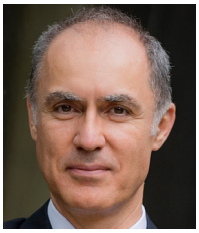

Miroslav Krstic is Distinguished Professor of Mechanical and Aerospace Engineering, holds the Alspach endowed chair, and is the Founding Director of the Cymer Center for Control Systems and Dynamics at UC San Diego. He also serves as Senior Associate Vice Chancellor for Research at UCSD. As a graduate student, Krstic won the UC Santa Barbara best dissertation award and student best paper awards at CDC and ACC. Krstic has been elected Fellow of seven scientific societies – IEEE, IFAC, ASME, SIAM, AAAS, IET (UK), and AIAA (Assoc. Fellow) – and as a foreign member of the Academy of Engineering of Serbia. He has received the ASME Oldenburger Medal, Nyquist Lecture Prize, Paynter Outstanding Investigator Award, Ragazzini Education Award, Chestnut textbook prize, the PECASE, NSF Career, and ONR Young Investigator awards, the Axelby and Schuck paper prizes, and the first UCSD Research Award given to an engineer. Krstic has also been awarded the Springer Visiting Professorship at UC Berkeley, the Distinguished Visiting Fellowship of the Royal Academy of Engineering, and the Invitation Fellowship of the Japan Society for the Promotion of Science. He serves as Senior Editor in IEEE Transactions on Automatic Control and Automatica, as editor of two Springer book series, and has served as Vice President for Technical Activities of the IEEE Control Systems Society and as chair of the IEEE CSS Fellow Committee. Krstic has coauthored thirteen books on adaptive, nonlinear, and stochastic control, extremum seeking, control of PDE systems including turbulent flows, and control of delay systems.